8

Advanced Harmonic Assessment

8.1 Introduction

Given the lack of detailed information normally available on the characteristics of the harmonic sources, the latter are often represented as approximate harmonic current injections. In an existing system these can be derived from selective measurements, whereas for planning studies the current injections are obtained from relatively simple models as described in Chapter 2.

In the static converter case the current injection method normally assumes a steady firing delay angle, either no commutation period or one of unvarying duration, an undistorted a.c. system voltage and perfect d.c. current. In practice this is rarely the case. Some voltage distortion and/or unbalance will exist on the a.c. side and current ripple on the d.c. side. Through the current controller the firing angle will not be steady and the commutation period duration will also vary. Therefore not only will harmonic voltages and currents be transferred through the converter, but they may also be amplified through the variation of the valves' switching instants. These interactions have particular relevance for non-characteristic harmonics.

Although the current injection method is used extensively in the design of filters, as explained in Chapter 6, this approach can lead to unsatisfactory solutions in applications involving very large power ratings such as an HVd.c. converter [1]. By ignoring or oversimplifying the interaction that exists between the converter and the a.c. and d.c. systems, an important low-order harmonic (or inter-harmonic) parallel resonance can be missed, leading to operational problems and even harmonic instabilities [2].

This chapter describes several algorithms with more advanced representation of the critical harmonic sources, taking into account their interactions with the rest of the power system components. Other topics discussed are the prospects for global harmonic state estimation and harmonic source identification. The chapter ends with a thorough assessment of the potential application of the electromagnetic transients simulation programs for harmonic analysis.

8.2 Transfer Function Model

Based on modulation theory and small signal linearisation, the transfer function concept provides an accurate direct solution of the converter response when the input voltage waveform is modulated by a signal at any specified frequency [3].

Power System Harmonics, Second Edition J. Arrillaga, N.R. Watson
 ISBN: 0-470-85129-5

In the case of the six-pulse converter, two transfer functions $Y_{\psi dc}$ and $Y_{\psi ac}$ are needed to describe the interconnection between the d.c. and a.c. sides of the converter. The d.c. voltage is calculated by summing each phase voltage multiplied by its associated transfer function, i.e.

$$v_d = N \sum_{\psi} Y_{\psi \mathrm{dc}} v_{\psi} \tag{8.1}$$

where $\psi = 0°$, $120°$ and $240°$ for phases a, b and c, N is the converter transformer ratio and v_{ψ} are the three phase voltages. $Y_{\psi \mathrm{dc}}$ has values between -1 and $+1$, where $+1$ signifies a connection of the d.c. side positive bus to the phase in question, -1 signifies a connection of the d.c. side negative bus to the phase in question, and 0 indicates no connection. By assigning the transfer function a value of 0.5 for the two commutating phases, the d.c. voltage is correctly represented during the commutation process.

The a.c. current in each phase can be defined by

$$i_{\psi} = N Y_{\psi \mathrm{ac}} i_{\mathrm{dc}} \tag{8.2}$$

where i_{dc} is the d.c. side current, and $Y_{\psi \mathrm{ac}}$ is similar to $Y_{\psi \mathrm{dc}}$, except that during the commutation period the a.c. current rises or falls in a continuous manner and is approximated by a linear transfer of the d.c. current from one phase to the next.

Both transfer functions are built up by the summation of a basic function (no commutation period and steady firing angle), a firing angle variation function, and a commutation function. The process is illustrated in Figure 8.1, where the dotted line represents the basic transfer function, the dashed line the function revised to include a firing angle variation of $\Delta\alpha$, and the solid line the function further revised to include the effect of a commutation period. Breaking up the transfer function in this way allows the frequency spectra to be more easily written.

The firing angle variation function is characterised as a set of pulses, with fixed leading edges and variable trailing edges. For $Y_{\psi \mathrm{dc}}$, the commutation function comprises a set of rectangular pulses, of which the leading edges match the firing angle variation, and the trailing edges vary somewhat differently. For $Y_{\psi \mathrm{ac}}$, the commutation function comprises a set of saw-tooth pulses, of which the leading and trailing edges match the firing angle variation. When the spectrum of this waveform is written, the current-time area of the commutation function has the dominant effect. An effective commutation period duration μ_1 is defined, such that the area of the $Y_{\psi \mathrm{dc}}$ commutation function matches the area of the true commutation waveform. In addition a small variable triangular pulse is added to account for the variation in this area consequential to the a.c. voltage, d.c. current, or firing angle variations.

The frequency spectra of the transfer functions is derived in Chapter 5 of reference [3].

The transfer function is a very useful concept for the design of control systems because it provides information on cause–effect relationships. However, to reduce the complexity of the formulation, the linearisation process is truncated at the first term of Taylor's series. This simplification has little effect on the accuracy of the results for the low harmonic orders but the solution accuracy decreases with increasing distortion magnitude and frequency.

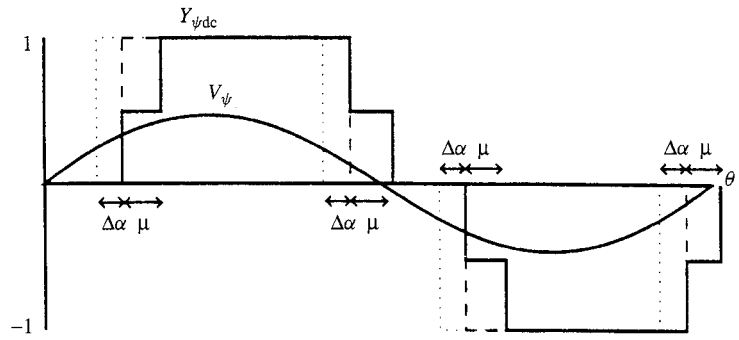

(a) Transfer function to d.c. voltage

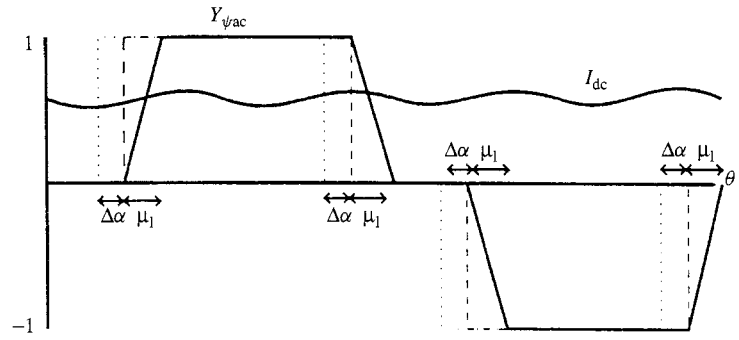

(b) Transfer function to a.c. current

Figure 8.1 Transfer functions: (a) $Y_{\psi dc}$; (b) $Y_{\psi ac}$

The main limitation of the direct solution is its inability to model the interaction between the harmonic source and the system harmonic flow.

8.3 Iterative Harmonic Analysis (IHA)

8.3.1 Fixed-Point Iterative Method

The simplest iterative scheme uses the fixed-point iteration (or Gauss) concept. At each iteration the latest values of the distorted terminal voltages are used to calculate the harmonic current injections. The direct analysis described in Chapter 7 is invoked to update the a.c. voltage harmonics for the next iteration. With reference to the three-phase static converter, the updated terminal voltages are used as the commutating voltages for the converter solution. The calculated d.c. voltage waveform is then impressed upon the d.c. side impedance to derive the d.c. current waveform, which in turn, together with the switching instants and commutation process, provides the a.c. current harmonic injections. The latter are then used to derive the a.c. voltage harmonics in the frequency domain for the next iteration.

Early fixed-point iterative methods involved the solution of the switching instants [4,5]. An alternative approach is to derive time-domain waveforms for the

direct voltage and a.c. side phase currents by evaluating analytical expressions for those quantities on a point-by-point basis and then applying the FFT to yield the desired harmonic information [6].

The fixed-point solution is likely to diverge when the d.c. system harmonic impedance is large and the commutating reactance small.

8.3.2 The Method of Norton Equivalents

In the fixed-point iteration, the nonlinear component is represented at each iteration by a constant current source. Far better convergence can be expected with the use of a Norton equivalent for the nonlinear component, with the Norton admittance representing a linearisation, possibly approximate, of the component response to variation in terminal voltage harmonics.

Time-invariant characteristics of some plant components, such as the transformer magnetisation, can be described by the static voltage–current relationship,

$$i(t) = f(v(t)) \tag{8.3}$$

in the time domain. In this case, the current injection and the Norton admittance can be calculated by an elegant procedure involving an excursion into the time domain [7]. At each iteration, the applied voltage harmonics are inverse Fourier transformed to yield the voltage waveform. The voltage waveform is then applied point-by-point to the static voltage/current characteristic, to yield the current waveform. By calculating the voltage and current waveform at $2n$ equi-spaced points, a fast Fourier transform (FFT) is readily applied to the current waveform, to yield the total harmonic injection. This process is illustrated in Figure 8.2 for the case of the transformer magnetisation nonlinearity.

8.3.3 Hybrid Time/Frequency Domain Solution

However, the characteristics of time-variant nonlinear components, such as power electronic devices, do not fall in the category defined by equation (8.3). Instead, their voltage–current relationships result from many interdependent factors, such as phase and magnitude of each of the a.c. voltage and current harmonic components, control system functions, firing angle constraints, etc. Moreover, the solution accuracy achieved with IHA methods when applied to static conversion is very limited due to the over-simplified modelling of the converters (in particular the idealised representation of the valve switching instants). The more accurate and generally applicable time-domain solution (such as the state variable or the EMTP method) has been proposed to represent the behaviour of the nonlinear components in a hybrid frequency/time domain solution [8,9].

The hybrid solution proceeds in two stages. First the periodic steady state of the individual components is derived from a load flow program and then updated using voltage corrections from the second stage. The calculations are performed in the frequency domain where appropriate (e.g. in the case of transmission lines) and in the

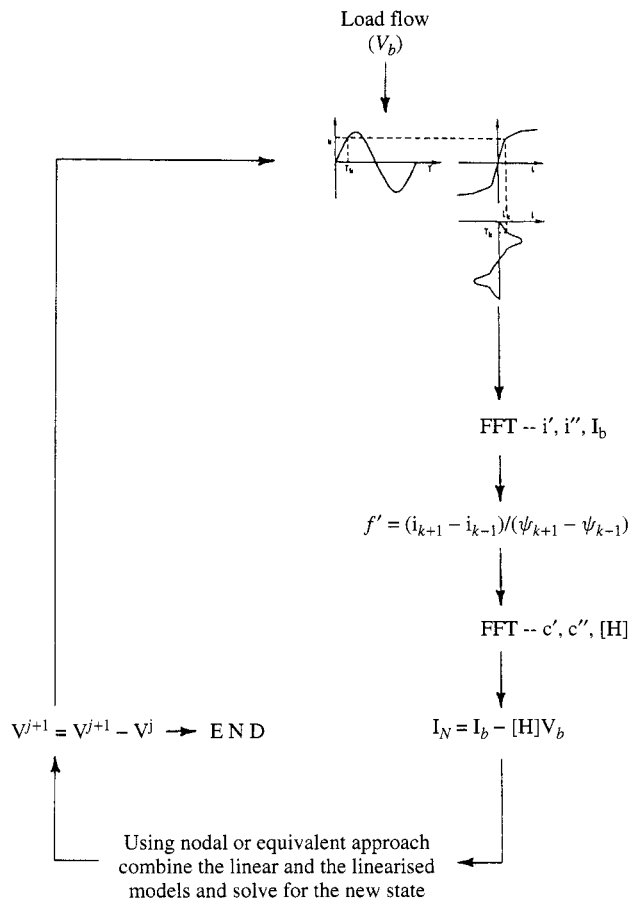

Figure 8.2 Iterative solution for the modelling of transformer magnetisation nonlinearities

time domain otherwise. In stage two the currents obtained in the first stage are used to derive the current mismatches Δi, expressed in the frequency domain. These become injections into a system-wide incremental harmonic admittance matrix Y, calculated in advance from such matrices for all the individual components. The equation $\Delta i = Y \Delta v$ is then solved for Δv to be used in the first stage to update all bus voltages.

The first stage approach is modular, but in the second stage the voltage corrections are calculated globally, i.e. for the whole system. However, convergence is only achieved linearly, because of the approximations made on the accuracy of Δv. A separate iterative procedure is needed to model the controllers of active nonlinear devices, such as a.c.–d.c. converters, and this procedure relies entirely on information from the previous iteration.

Acceleration Technique Time-domain simulation, whether performed by the EMTP, state variable or any other method, may require large computation times to reach steady state, thus the use of accelerating techniques [10,11] is advocated to speed up the solution. These techniques take advantage of the two-point boundary value inherent in

the steady-state condition. Thus a correction term is added to the initial state vector, calculated as a function of the residuum of the initial and final state vectors and the mapping derivative over the period. A concise version of the Poincare method described in reference [11] is given here.

A nonlinear system of state equations is expressed as

$$\dot{x} = g(x, u) \qquad x(t_o) = x_o \tag{8.4}$$

where $u = u(t)$ is the input, and x_o the vector of state variables at $t = t_o$ close to the periodic steady state. This state is characterised by the condition

$$f(x_o) = x(t_o + T) - x(t_o) \tag{8.5}$$

where $x(t_o + T)$ is derived by numerical integration over the period t_o to $t_o + T$ of the state equations (8.4).

Equation (8.5) represents a system of n nonlinear algebraic equations with n unknowns x and can thus be solved by the Newton–Raphson method.

The linearised form of equation (8.5) around an approximation $x_o^{(k)}$ at step k of its solution is

$$f(x_o) \cong f(x_o^{(k)}) + J^{(k)}(x_o^{(k+1)} - x_o^{(k)}) = 0 \tag{8.6}$$

where $J^{(k)}$ is the Jacobian (the matrix of partial derivatives of $f(x_o)$ with respect to x_o, evaluated at $x_o^{(k)}$).

With

$$x_o^{(k)} \rightarrow f(x_o^{(k)}) \tag{8.7}$$

and

$$x_o^{(k)} + \varepsilon e_i \rightarrow f(x_o^{(k)} + \varepsilon e_i) \quad i = 1, \ldots, n \tag{8.8}$$

where e_i are the columns of the unity matrix and ε is a small scalar, the $J^{(k)}$ is assembled from the vectors

$$\frac{1}{\varepsilon}(f(x_o^{(k)} + \varepsilon e_i) - f(x_o^{(k)})) \quad i = 1, \ldots, n \tag{8.9}$$

obtained in equations (8.7) and (8.8).

Finally, using the above approximation $J^{(k)}$ of the Jacobian, the updated value $x_o^{(k+1)}$ for x_o is obtained from equation (8.6).

The process described above is quasi-Newton but its convergence is close to quadratic. Therefore, as in a conventional Newton power flow program, only three to five iterations are needed for convergence to a highly accurate solution, depending on the closeness of the initial state x_o to the converged solution.

8.3.4 The Harmonic Domain

An important step in solution accuracy and reliability is provided by the so-called harmonic domain [12], a full Newton solution that takes into account the modulating

effect of a.c. voltage and d.c. current distortion on the switching instants and converter control functions. This method performs a linearisation around the operating point, that provides sufficient accuracy. Modelling a distorting source in the harmonic domain requires the derivation of a set of nonlinear equations describing the harmonic transfer through the device in the steady state. A different model is thus required for each nonlinear device.

So far this method has been applied to three-phase static power conversion equipment. The converter model must be differentiable with respect to the solution variables and this is achieved by the convolution technique, which calculates the transfers analytically using easily differentiable real-valued functions. The advantage of describing the system in real-valued terms is that both electrical and non-electrical variables, such as control variables, can be solved simultaneously.

Each of the six-pulse bridges of a converter terminal can be viewed as a four-port circuit, i.e. consisting of two inputs and two outputs. The inputs in this case are the a.c. phase voltage spectra and the d.c. current spectra. The outputs are the a.c. current and d.c. voltage spectra. The convolution technique approximates the transferred waveshapes (d.c. voltage and a.c. phase currents) to piece-wise waveshapes consisting of twelve distinct periods of conduction. These periods are defined explicitly by the switching angles of the converter. In the case of the d.c. voltage transfer, twelve analytic frequency-domain expressions are derived from nodal analysis of the twelve commutation circuits which describe steady-state waveshapes valid for those circuits. The spectra calculated using these expressions are then convolved with those of band-limited rectangular windowing functions. The resultant sum of the convolved spectra is that of the total waveshape. Figure 8.3 illustrates one convolution for the d.c. voltage of an inverter as seen in the time domain.

A similar process is followed to obtain the harmonic spectra of the a.c. phase currents. These transfers are general for both inverter and rectifier, with only the direction of d.c. current flow and the resultant sign of the d.c. voltage across the bridge being different.

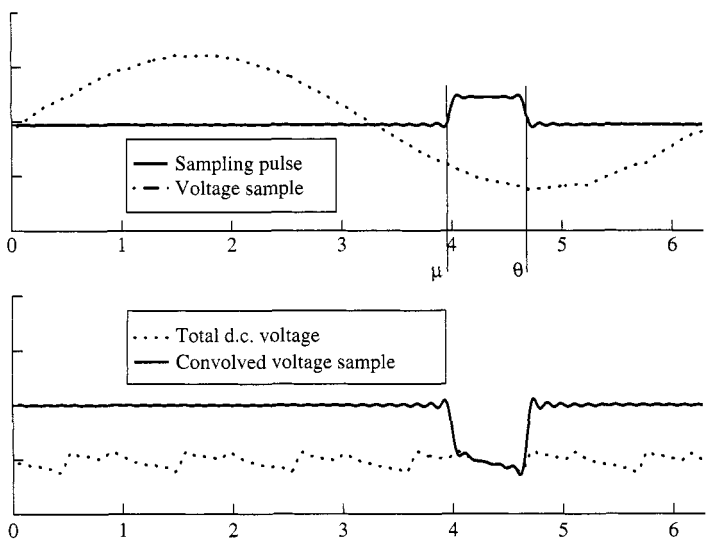

Figure 8.3 Convolution sampling waveforms for a six-pulse converter

The harmonic transfers across a converter are largely dependant upon the accuracy of determining the switching instants, particularly the end of commutation angle. For the convolution model these angles are obtained from twelve single-variable Newton–Raphson steps. The commutation angles are defined by the cross-over points of the commutation currents with the d.c. current (harmonics included). The firing angles are dependant upon the control strategy but are also solved using single-variable iterative steps. As the full solution Jacobian includes the effect of modulating these switching instants, the main solution is still of a full Newton nature.

To solve the standard twelve-pulse configuration, two convolution models are needed for the star/star and star/delta connected bridges. The harmonic transfers from each model are added together to yield the full transfer characteristic.

Each frequency is ordered by phase components and is partitioned into real and imaginary parts. This leads to six variables for each harmonic at an a.c. busbar, and two at a d.c. busbar. Consequently, for a study to the 50th harmonic, 300 variables need to be defined at the converter a.c. terminal and 100 at the d.c. terminal. The remaining required mismatches are those for the average d.c. current and the control variables. For a current-controlled rectifier these are the firing angles, which are modulated by the d.c. current through a PI (proportional integral) controller. The minimum gamma controlled inverter assumes equidistant firings but requires the commutating voltage zero crossings as variables in order to calculate the extinction angles.

The Jacobian, in Newton's solution, only needs to be approximate, and therefore only the significant terms need to be retained. Thus the full harmonic Jacobian can be about 96% sparse without affecting convergence. The Jacobian elements can be calculated either by numerical partial differentiation or by analytically derived expressions for the partial derivatives. Numerical calculation of the Jacobian has the advantage of ease of coding, but is very slow; it is achieved by sequentially perturbing each variable and calculating the change in all the mismatches. The analytical method of calculating the Jacobian matrix requires considerable effort to obtain all the partial derivatives in analytic form, but is exceptionally fast. Thus the latter method is preferred because the solution speed is increased by a factor of 50 with respect to using one obtained numerically.

Good variable initialisation is achieved in a two-stage process. The first stage uses a positive-sequence power flow estimation and classical converter equations. This information is used to start a three-phase power-flow solution including the control variables; the results of the latter are then used to initialise the full harmonic solution.

As the two converters of an HVd.c. link interact nonlinearly with each other, it is necessary to solve them simultaneously. At each converter busbar the variables represent the specified harmonics in ascending order. The structure of the Jacobian is illustrated in Figure 8.4, although for simplicity it only includes 13 harmonics.

The two a.c. systems of the d.c. link are not directly connected, and therefore there is no direct coupling between the two a.c. busbars represented by numbers 1 and 2. This can be seen in the matrix by the presence of zero blocks A2 and B1. The two d.c. busbars at 3 and 4 are directly coupled through the nodal analysis of the system; blocks C4 and D3 are the diagonal linear linking elements.

Some refinements have been made to the harmonic domain algorithm to make it suitable for the efficient computation of inter-harmonics [13]. Inter-harmonics can be accommodated efficiently by means of an adaptive technique complemented by

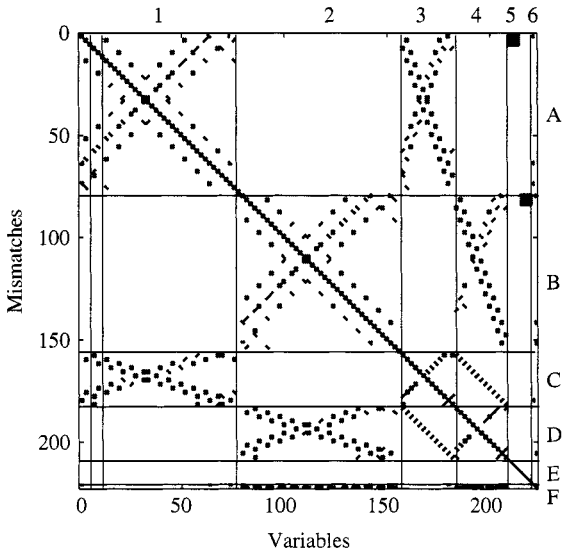

Figure 8.4 Jacobian of the CIGRE Hvd.c. test system for 13 harmonics

interpolation between integer frequencies [14]. These refinements take advantage of the inherent sparsity present in the harmonic arrays, which provide several orders of improvement in solution time with no significant degradation in solution accuracy. As a result, the increase in computation is now almost linear with the number of power frequency cycles, as opposed to cubic with the original full method.

Although in principle any type of nonlinear component can be accommodated in the harmonic domain solution, the formulation of each new component requires considerable skill and effort. Accordingly, a program for the calculation of the non-sinusoidal periodic steady state may be of very high dimension and complexity, as well as being difficult to use and develop further. However, this method is extremely useful to assess the harmonic interaction between a.c. system and large power converters and has already been adopted by several large manufacturers.

8.4 Harmonic Power Flow

The concept of harmonic power flow (HPF) was introduced in an early contribution by Xia and Heydt [15] for the case of a symmetrical power system. Although there have been further publications discussing this subject in the three-phase frame of reference [16–19], most of the power quality contributions still use the HPF concept with exclusive reference to symmetrical operation on the basis that at the fundamental frequency the power system is designed to operate under strict limits of unbalance. However, the symmetrical solution is of very limited value to the industry because the experience of many field tests indicates that asymmetry is the rule rather than the exception with power system harmonics (both at characteristic and non-characteristic harmonic frequencies) and such information can not be represented in a balanced HPF.

Further compelling reasons for replacing the symmetrical HPF concept by the three-phase alternative are:

(1) System unbalance produces non-characteristic harmonics in power electronic equipment, particularly non-zero-sequence triplens. These are not normally filtered and penetrate into the a.c. network regardless of the type of transformer connection.
(2) Often the filters of large power conversion plant resonate with the a.c. system impedance at low-order non-characteristic harmonics such as the third.
(3) Transmission system unbalance is greatly affected by line geometry, and the use of transpositions, calculated to reduce fundamental frequency imbalance, is ineffective at harmonic frequencies [20].
(4) Harmonic flows are affected by the transformer connections, which only a three-phase model can represent.
(5) The need to model harmonic interactions between geographically separated converter units.

The derivation of voltage inbalance requires a three-phase power flow solution. With this information a three-phase model of the converter plant derives the characteristic and non-characteristic harmonic currents injected by the converter, which constitute the exciting sources for the harmonic penetration model described in Chapter 7.

Generally a direct solution based on the inbalance calculated from a preliminary three-phase power flow will provide sufficiently accurate information. A few sequential iterations of the three-phase power flow and the harmonic penetration study may be required for greater accuracy [16].

However, under difficult resonant conditions the sequential solution is likely to diverge and a unified Newton solution provides a more reliable alternative.

8.4.1 Components of a Three-Phase Newton HPF Solution

The three constituent parts of an HPF for use in systems containing large power converters are:

(1) a three-phase a.c.–d.c. power flow [21] at the fundamental frequency;
(2) a multi-harmonic three-phase representation of the linear part of the power system (the subject of Chapter 7);
(3) a harmonic domain representation of the individual converters, as described in Section 8.3.4.

These three components need to be coupled with each other in a large, mostly block-diagonal, Jacobian matrix.

Power Flow Requirements Unification of the three-phase power flow and harmonic interaction at the converter terminals imposes a different set of requirements on the power flow implementation than those that led to the development of the decoupled algorithms. First, the converter harmonic model is necessarily in Cartesian

co-ordinates [22]. If the power flow equations are in polar co-ordinates, as required by the decoupling concept, nonlinear polar transforms must be carried out at each iteration to interface with the converter a.c. terminal (at fundamental frequency). This is likely to increase the number of iterations to convergence substantially, as well as complicate the power flow implementation. An additional factor to consider is that the converter equations take longer to calculate than the solution of the prefactorised Jacobian system. It is therefore desirable to reduce the number of converter mismatch equation evaluations by reducing the number of iterations to convergence. This can be achieved by using the full Jacobian matrix, with no decoupling. Taken together, these points indicate that a unified power flow and harmonic solution in Cartesian co-ordinates will be more efficient than one in polar co-ordinates.

Combined Jacobian The nine-busbar network of Figure 8.5 is used to illustrate the structure of the combined power flow and harmonic solution. The slack busbar is at ROXBURGH-011, and loads are placed at ROXBURGH-220, INVERCARG-011 and TIWAI-220. Also, the rectifier end of the CIGRE benchmark model [23] is connected at the TIWAI busbar.

The combined Jacobian is illustrated in Figure 8.6. In this figure, the busbars and specifications of the power flow solution can be observed at the top left-hand side. Of

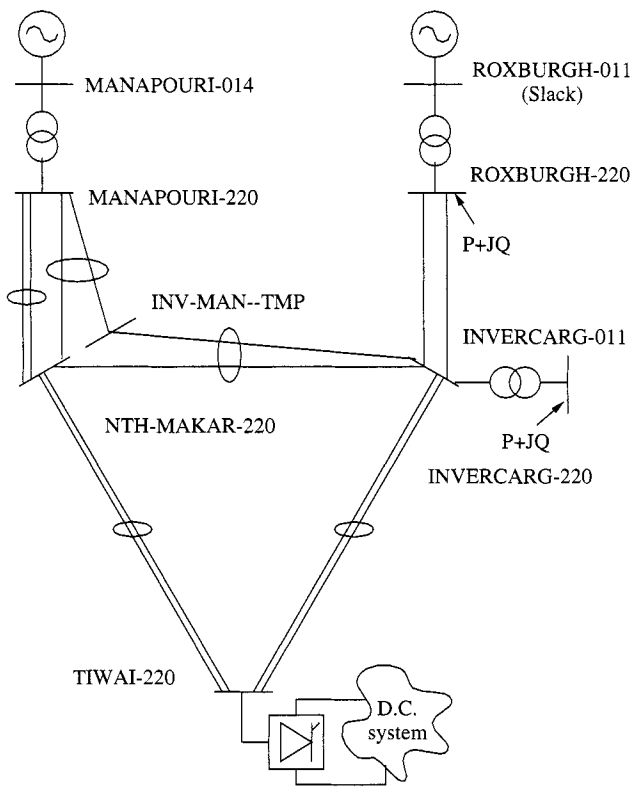

Figure 8.5 Test system for three-phase power flow

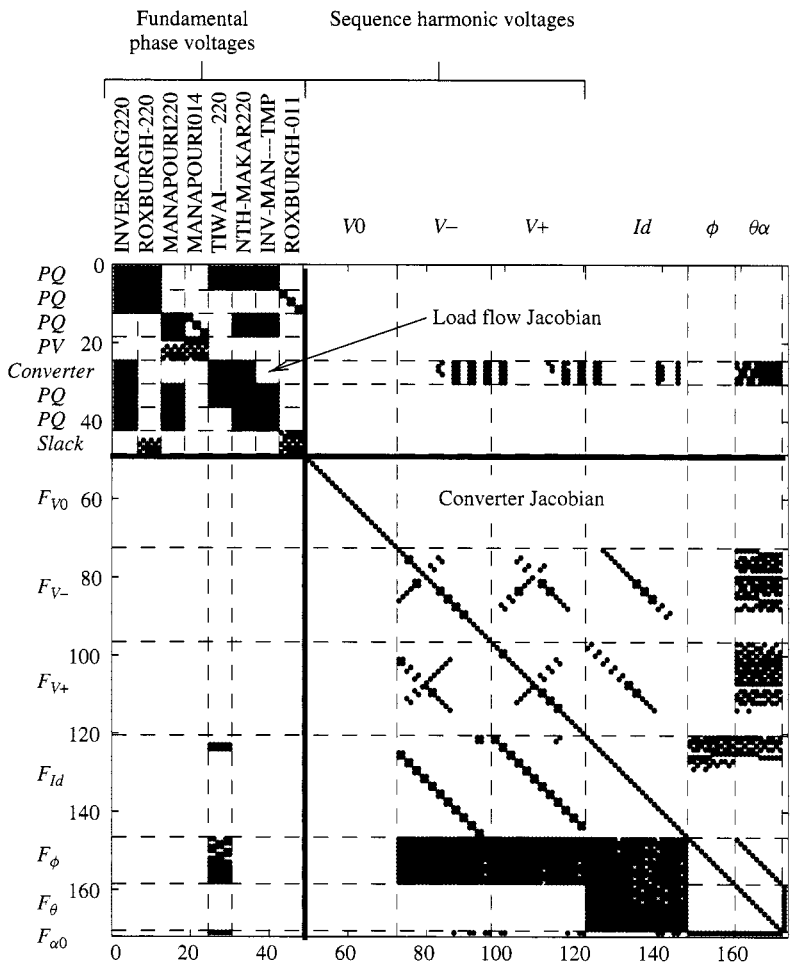

Figure 8.6 Jacobian matrix for an integrated power flow and harmonic solution

course, the structural sparsity would be much greater for a realistically sized system, and is clearly not symmetric. The lower right-hand side matrix block represents the converter harmonics solution, which is seen to be coupled only to the fundamental frequency voltages at the converter terminals.

The combined Jacobian contains no more terms than the separate Jacobians of the load flow and converter, and yet convergence has been found to be faster and more robust than a fixed-point iteration between separate load flow and converter model updates, which usually diverges.

The Thevenin equivalent of the a.c. system is retained at all harmonic frequencies except the fundamental, which is the point of coupling to the power flow equations. Similarly, three-phase power flow equations are retained at every bus except the converter bus. It is assumed that were it not for the converter, the converter bus would be *PQ* specified. Since the power flow is three-phase, six mismatch equations (real and imaginary parts) are required at the converter bus at fundamental frequency.

Because the processing required at every iteration is dominated by the converter equations, it is essential that convergence of the load flow part of the system be faster than that of the converter model, which typically converges in seven iterations. The decoupled load flow method is not suitable as it requires more iterations for convergence. As explained above, integration of the converter model with a load flow requires that the load flow be reformulated in Cartesian components, with no decoupling in the Jacobian matrix.

General HPF Framework for Systems with Multiple Converters The method and components of the Newton solution have already been discussed in previous sections with reference to a single 12-pulse converter connected to an a.c. power system. This section describes the structure of a general Jacobian capable of accommodating, as well as a three-phase power flow, multiple converters of different pulse numbers and d.c. configurations placed in separate locations.

While all the system busbars must be explicitly represented at the power frequency, due to the nonlinear nature of the power flow specifications, only the converter busbars are nonlinear at the harmonic frequencies. Thus, in the latter case, the linear network can be reduced to an equivalent system that links the nonlinear device busbars. The linear reduction used also produces equivalent current injections for remote constant voltage or current harmonic sources.

By way of illustration, Figure 8.7 shows the structure of the Jacobian representing the power and harmonic flows in the New Zealand South Island transmission system. This system consists of 100 busbars, of which 14 are generation busbars, 24 *PQ* loads and 4 large rectifier busbars. The total system loading is about 2500 MW, of which over half is rectified. Consequently there has been a question mark over the degree of interaction between the four rectifier busbars (shown in Figure 8.8).

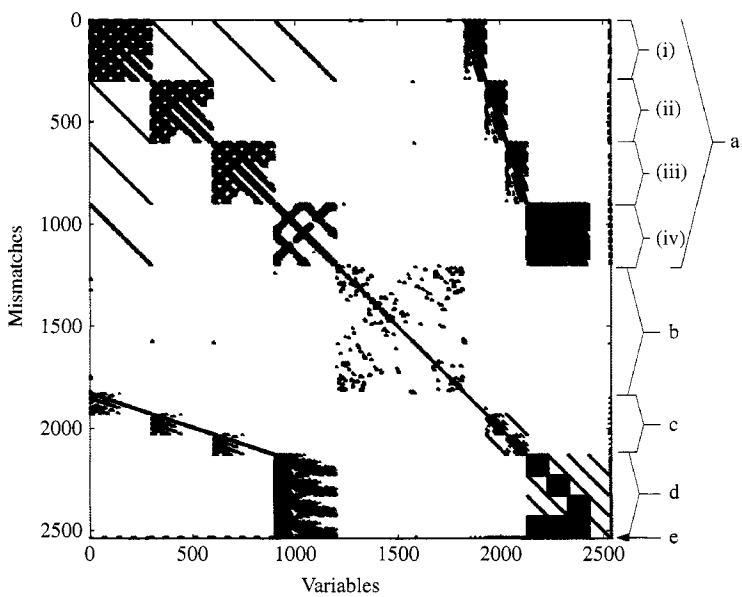

Figure 8.7 Jacobian structure of the New Zealand South Island system

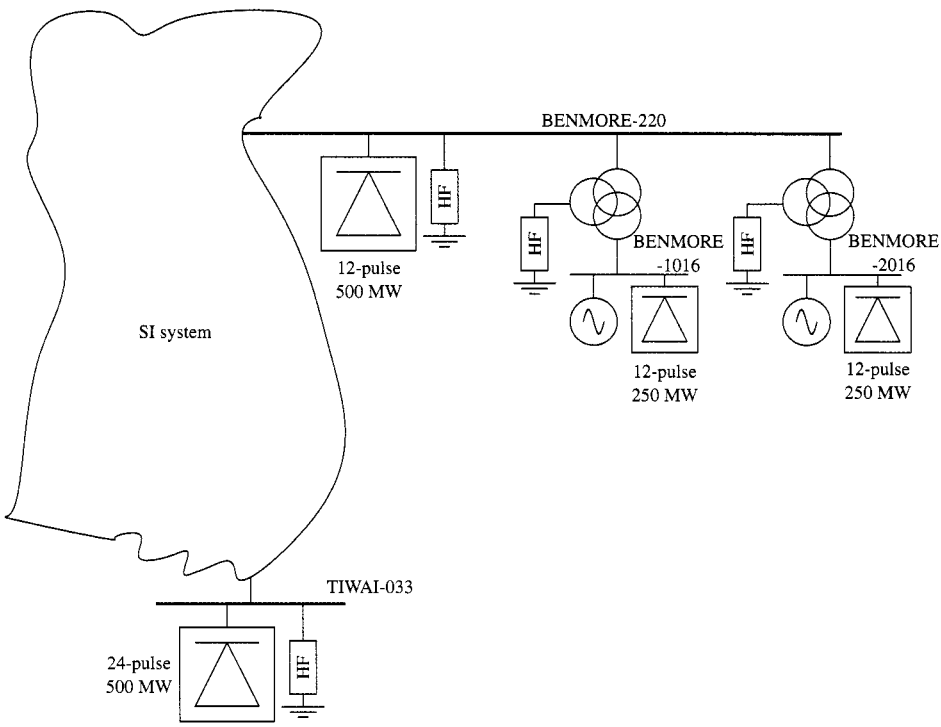

Figure 8.8 Multiconverter system (New Zealand South Island)

Three of the busbars are grouped together at Benmore in the middle of the South Island and form one end of the 1000 MW bipolar HVd.c. link. The fourth is located at Tiwai, at the southern end of the South Island, and is a 500 MW aluminium smelter.

As explained in Section 8.3.4, 426 variables and mismatches are needed at each converter bus, consisting of 300 a.c. voltages and 100 d.c. currents, the remaining 26 being switching and control terms. These three components are separated in the generalised Jacobian, as shown in Figure 8.7, where all the switching terms are placed last.

The 300 × 300 uppermost diagonal block contains the Benmore converter a.c. voltage variables and mismatches. Similarly, the next block diagonal matrix (also of order 300 × 300) contains the a.c. voltages of the Tiwai converters. The remaining elements in the upper left-hand side region represents the couplings (harmonic interactions) between the Benmore and Tiwai converters. Further down, and also on the right, are the (100 × 100) d.c. current harmonic terms and their coupling elements to the rest of the converter variables. The low right-hand side matrix contains the elements of the three-phase power flow (100 buses × 3 phases × 2 real and imaginary parts). Finally, the bottom and far right parts of the Jacobian contain the relatively few switching and control terms (26 per converter).

The test system is used to assess the ability of the unified algorithm to determine the degree of interaction between the multiple converters. At light load the Benmore-220 filters are normally out of service to minimise excessive VAR generation. Under these conditions, the results of the unified algorithm, shown by the black trace in Figure 8.9, are considerably different than those of the simplified model; this indicates

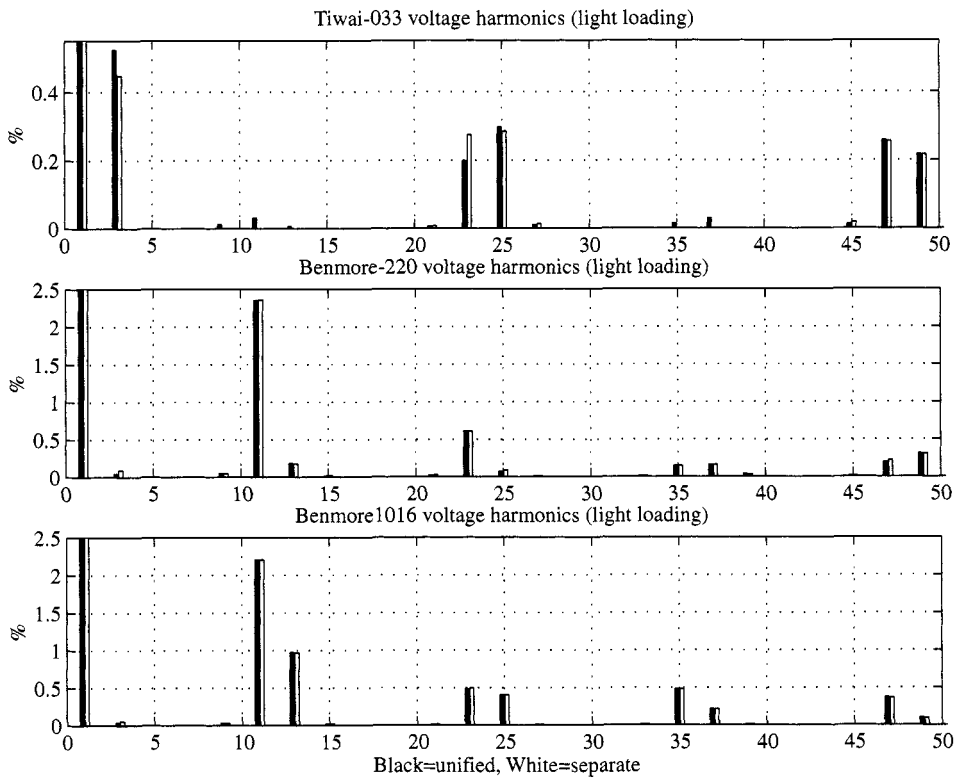

Figure 8.9 Comparison of harmonic voltages with the Benmore filters out of service

that in this case there is a noticeable harmonic interaction between the Tiwai-033 and Benmore converters.

8.5 Harmonic State Estimation

Recent contributions [24–33] have extended the concept of power system state estimation to harmonic frequencies. However, full measurement of the system states, by first recording the voltage and current waveforms at nodes and lines and then deriving their frequency spectra, is prohibitive for a large system. Only partial measurement (not necessarily made at the harmonic sources) is practical and, therefore, the measurements must be complemented by system simulation.

The framework of harmonic state estimation is illustrated in Figure 8.10. It uses a three-phase system model to describe asymmetrical conditions such as circuit mutual couplings, impedance and current injection unbalance. A partial measurement set is also needed consisting of some bus voltages, injection currents and line currents, or bus injection volt-amperes and line volt-amperes. Instead of system-wide harmonic state estimation, some contributions [34,35] discuss the issue with reference to the estimation of the harmonic components from the voltage or current waveform at a measurement point.

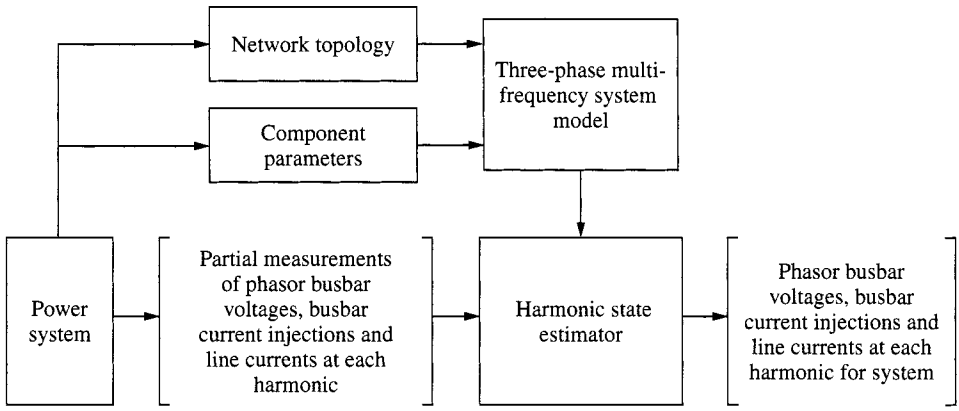

Figure 8.10 Framework for harmonic state estimation

Based on the network topology, a harmonic state estimator (HSE) is formulated from the system admittance matrix at harmonic frequencies and the placement of measurement points. Measurements of voltage and current harmonics at selected busbars and lines are sent to a central workstation for the estimation of bus injection current, bus voltage and line current spectra at all or selected positions in the network.

The placement of measurement points is normally assumed symmetrical (e.g. either three or no phases of injection currents of a busbar are measured). However, this requirement restricts the search for optimal placement of measurement points in three-phase asymmetrical power systems.

The implementation of existing algorithms is in practice limited by poor synchronisation of conventional instrumentation schemes, lack of continuity of measurements or lack of processing speed. A system-wide or partially observable HSE requires synchronised measurement of phasor voltage and current harmonics made at the different measurement points, as illustrated in Figure 8.11.

HSE turns multi-point measurement to *system-wide measurement* in a very economic way. Two important optimisation problems in HSE are the maximum observable subsystem for a given measurement placement, and the minimum number of measurement channels needed for the observability of a given system. The HSE can be implemented continuously in real time if the measurement is continuous and the processing speed fast enough. Potentially, the harmonic monitoring instrument and estimator can be integrated into an existing supervisory control and data acquisition (SCADA) system.

State estimation is thus an alternative, or a supplement, to the direct measurement of electrical signals. Strictly speaking, a system state is a mathematically definable, although not necessarily measurable, electrical quantity such as a nodal voltage or a line current. In practice, however, the *state* concept is often extended to other variables, such as the voltage phase angle difference of a transmission line; it is also used for complex combinations of individual variables.

The task of the HSE is to generate the 'best' estimate of the harmonic levels from limited measured harmonic data, corrupted with measurement noise. The three issues involved are the choice of state variables, some performance criteria and the selection of measurement points and quantities to be measured.

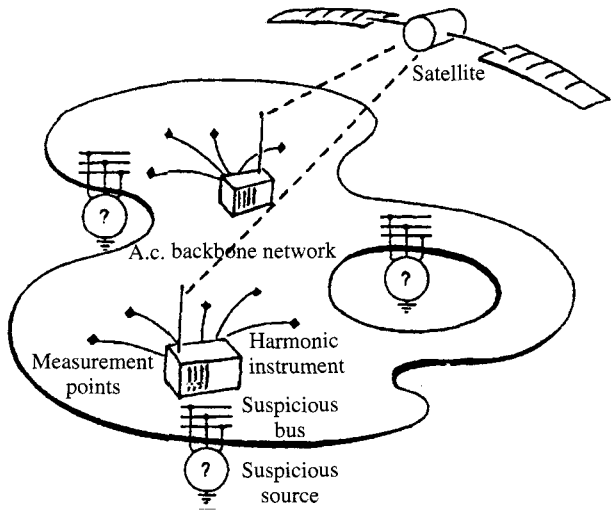

Figure 8.11 System-wide harmonic state estimation

State variables are those variables that, if known, completely specify the system. The voltage phasors at all the busbars are usually chosen, as they allow the branch currents, shunt currents and currents injected into the busbar to be determined.

Various performance criteria are possible, the most widely used being the weighted least-squares (WLS)

Observability analysis (OA) [29] is required in HSE to identify its solvability. A power system is said to be observable if the set of available measurements is sufficient to calculate all the state variables of the system uniquely. Observability is dependent on the number, locations and types of available measurements, and the network topology, as well as the system admittance matrix. For a different network topology, or the same network topology but different measurement placements, an OA is to be performed in each case.

It is important for OA not only to decide whether the system is observable and hence system-wide HSE can be performed, but also to provide information about the observable/unobservable islands as well as redundant measurement points if not completely observable. This allows the repositioning of measurement points to maximise their usefulness.

A system is observable if a unique solution can be obtained for the given measurements. A unique solution exists if and only if the rank of $[h]$ equals the number of unknown state variables. Therefore, for observability the number of measurements must not be less than the number of state variables to be estimated. However, this condition is not sufficient since linear dependency may exist among rows of the measurement matrix. The rank of $[h]$ does not depend on the quality of the measurements and therefore the noise vector can be assumed to be zero.

Existing OA can be divided into three groups of methods: numerical (floating-point calculations), topological and symbolic. A detailed coverage of this topic is made in [24,25].

8.5.1 Load and Harmonic Source Identification

The harmonic simulation and HSE algorithms differ regarding the way loads are treated. In general, a load bus may contain linear (passive) and nonlinear components. These can be modelled in detail in harmonic simulation, which represents separately the current injections and the passive components. HSE, on the other hand, may have no information about the composition of the load and is only capable of estimating the net current flow into or out of the load busbar.

Therefore, the current injection information supplied to the HSE algorithm is the sum of the harmonic current source and harmonic current flowing in the load. The harmonic voltages at the suspicious buses, and harmonic currents injected from the suspicious sources to the backbone, are provided by the estimator at the end of HSE and each suspicious source is classified as a harmonic injector or a harmonic absorber.

In general, a suspicious harmonic source can be considered as a Norton equivalent circuit at each harmonic frequency (Figure 8.12), and the following relationship applies for a harmonic of order n:

$$\hat{I}_i(n) - I_i(n) = V_i(n)\ Y_i(n) \tag{8.10}$$

In equation (8.10), $V_i(n)$ and $I_i(n)$ are the nodal voltage and current injection, respectively, as provided by the estimator, while $\hat{I}_i(n)$ and $Y_i(n)$ are the unknown Norton harmonic current injection and admittance within the suspicious source ($i = 1, 2, 3$). In theory, it should be possible to derive some information on the nature of the load from the estimated harmonic voltages and injected currents at the bus.

When no harmonic current injection exists at a node, it is possible to identify the load impedance using the nodal harmonic voltage and current information at two different harmonics. This calculated impedance can be verified using information at other frequencies. When a harmonic source is present, it is not possible to identify the components without additional information. This information may come from measurements obtained under different operating conditions (e.g. a component switched in or out)

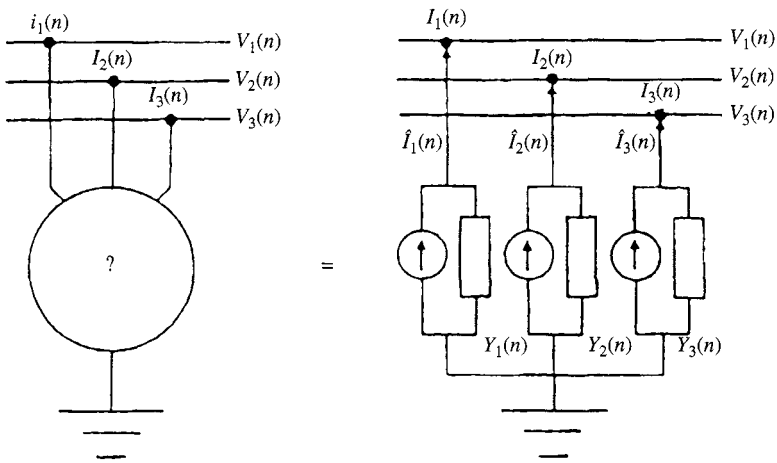

Figure 8.12 Norton equivalent for suspicious harmonic sources

or may take the form of an assumed ratio of the harmonic current injection to the fundamental based on the converter pulse number. In the latter case, if the following two assumptions are made for the suspicious source,

$$Y_i(n) = G_i - j\ B_i/n \tag{8.11}$$

$$|\hat{I}_i(n)| = \delta_i(n, n_0)|\hat{I}_i(n_0)| \tag{8.12}$$

where G_i and B_i are unknown parameters for node i, n_0 is a chosen reference harmonic (e.g. the 11th harmonic for the cases of 6-pulse and 12-pulse converters), and $\delta_i(n, n_o)$ is a chosen ratio of $|\hat{I}_i(n)|$ to $|\hat{I}_i(n_0)|$, then for any two harmonics n_1 and n_2 which are not n_0, the set of quadratic equations (equations (8.10)–(8.12)) is solvable to obtain the unknown Norton parameters $\hat{I}_i(n)$ and $Y_i(n)$ for each harmonic n of interest.

It can be shown, by sensitivity analysis, that the estimated Norton parameters using the above method are very dependent on the chosen ratio when the suspicious source contains non-zero Norton current injections, and very insensitive to the chosen ratio when the suspicious source does not contain Norton current injections. Therefore, the above method can at least be used to identify whether a suspicious source is a purely passive load and, in such case, estimate the equivalent harmonic admittances of the passive load.

8.6 The Electromagnetic Transients Solution

The EMTP method, although designed for the simulation of transients, can also be used for the derivation of the steady-state voltage and current waveforms taking into account the variety of system nonlinearities and the effect of the control functions. Its potential extension to the steady-state solution should therefore simplify the calculation of power system harmonics. Two different modelling philosophies have been proposed for this purpose. One is the hybrid solution outlined above, which is basically a frequency-domain solution with periodic excursions into the time domain to update the contribution of the nonlinear components. The alternative is a basically time-domain solution to the steady state followed by FFT processing of the resulting waveforms. The latter alternative offers greater user simplicity, given the general availability of EMTP packages, and is thus described further in the remaining part of the chapter.

Starting from standstill, the basic time domain uses a 'brute force' solution, i.e. the system equations are integrated until the steady state is reached within a specified tolerance. The voltage and current waveforms, represented by sets of discrete values at equally spaced intervals (*corresponding* with the integration steps), are subjected to FFT processing to derive the harmonic spectra. This is a very simple method but can be slow when the network has components with light damping.

The use of acceleration techniques, described in Section 8.3.3 for the hybrid solution, is not recommended here for the following reason. The number of periods to be processed in the time domain required by the acceleration technique is almost directly proportional to the number of state variables multiplied by the number of Newton iterations. Therefore the solution efficiency reduces very rapidly as the a.c. system size increases. This is not a problem in the case of the hybrid algorithm, because in that

case the time-domain solutions require no explicit representation of the a.c. network. On the other hand, when the solution is carried out entirely in the time domain, the a.c. system components are included in the formulation and thus the number of state variables is always large. Moreover, as the time-domain algorithm requires only a single transient simulation to steady state run, the advantage of the acceleration technique is questionable in this case, due to the additional complexity.

This method is very easy to use given the general availability of EMTP packages with flexible and detailed modelling of the nonlinear components. However, their accuracy is limited by the restricted frequency-dependence representation of the a.c. system components, although this problem can be greatly reduced with the use of frequency-dependent equivalents for the linear part of the system (a subject described later in this section).

8.6.1 Time Step Selection

The time step selection is critical to model accurately the resonant conditions when converters are involved. A resonant system modelled with 100 μS or 50 μS steps can miss a resonance, while the use of a 10 μS does not. Moreover, the higher the resonant frequency the smaller the step should be. A possible way of checking the effectiveness of a given time step is to reduce the step and then compare the results with those obtained in the previous run. If there is a significant change around the resonant frequency, then the time step is too large. The main reason for the small time step requirement is the need to pin-point the commutation instants very accurately, as these have great influence on the positive feedback that appears to occur between the a.c. harmonic voltages and the corresponding driven converter currents.

8.6.2 A.C. System Representation

The main requirement of a harmonic solution is the use of an accurate frequency-dependent model for the system components. This is best achieved in the frequency domain and has been the main reason for the development of the hybrid algorithms.

The next important question is the size of detailed system representation. To illustrate this point, Figure 8.13 shows the effect of the extent of system representation on the harmonic impedances. The solid line indicates a representation of the entire transmission system (11 kV and above) of the New Zealand South Island system. The dash-dotted line relates to a system reduced down to the local 220 kV network and only significant loads and generators represented. The dashed line represents the case of the 220 kV transmission network without generators, transformers or loads. The differences between these cases are very pronounced.

8.6.3 Frequency-Dependent Network Equivalents

The use of a frequency-dependent network equivalent (FDNE) avoids the need to model any significant part of the a.c. system in detail, yet can still provide an accurate picture of the system impedance across the selected range of harmonic frequencies.

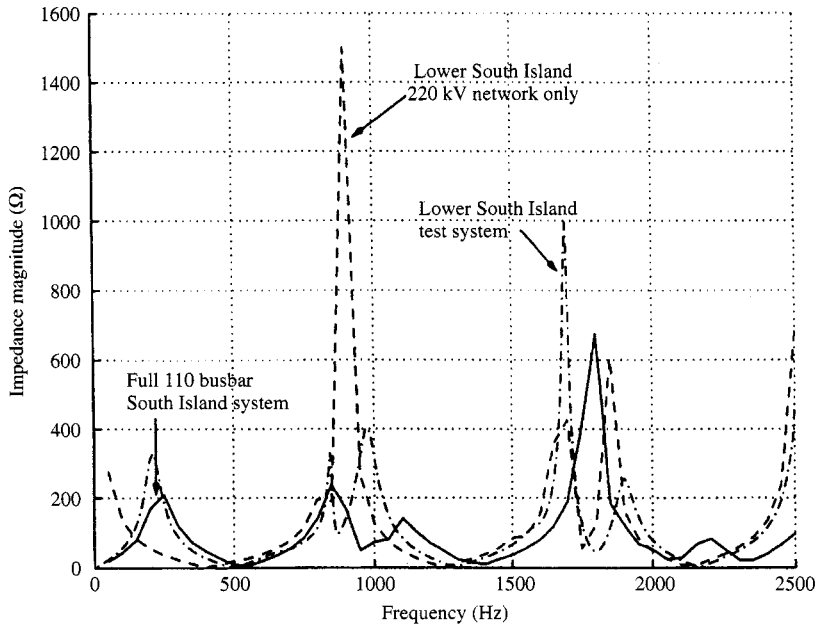

Figure 8.13 Comparison of depth of system representation

An early proposal [36] used the resonant points of the network frequency response to derive a set of tuned branches that can be easily incorporated into the EMTP program. Although the synthesis of those branches is direct, this method first ignores the losses to determine the L and C values for the required resonant frequencies and then determines the R values to match the response at minima points. In practice an iterative optimisation procedure is necessary after this process to improve the fit.

The equivalents of multiterminal circuits, such as a three-phase system with mutual couplings between phases, requires the fitting of admittance matrices instead of scalar admittances [37].

A criticism of the above technique for general transients use is that it can not model an arbitrary response. An alternative approach is to fit a rational function to a response and implement it directly in the transients program without the need for an equivalent circuit. In the latter, however, the parameters are functions of the time step and hence the fitting must be performed again when the time step is altered. Moreover the stability of the fit, without which the system can not be simulated, is still a problem with the rational function methods. Thus the parallel branches *RLC* equivalent provides greater simplicity and reliability at the expense of accuracy over the rational function methods. For (steady state) harmonic studies, where transient performance is not an issue, the parallel branches *RLC* equivalent can be fitted with high Q tuned branches for each harmonic, giving good accuracy at each harmonic but not at intermediate frequencies.

8.6.4 Case Study

The application of FDNE to harmonic analysis is illustrated here with reference to the CIGRE benchmark link [23] with the rectifier a.c. system replaced by the New Zealand

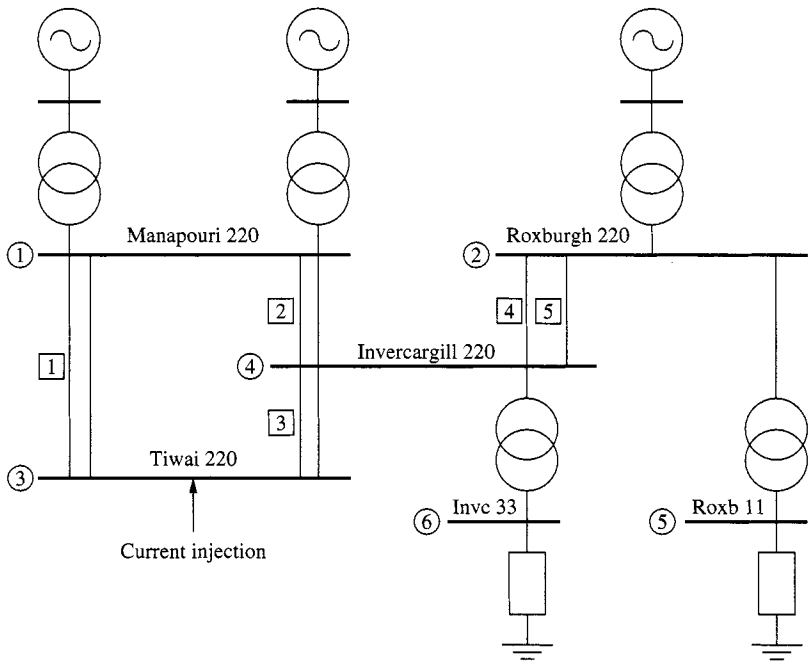

Figure 8.14 Lower South Island of New Zealand

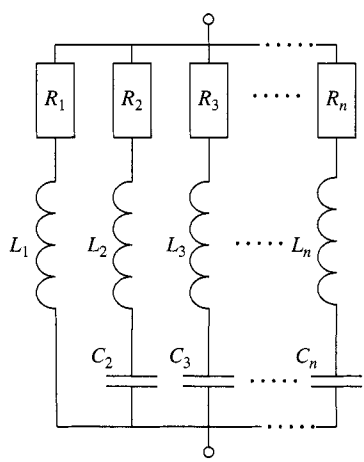

Figure 8.15 *RLC* network

Lower South Island test system [3] (Figure 8.14), which will be represented by a frequency-dependent network equivalent with the admittance terms emulated either by rational functions in the z domain or parallel *RLC* branches (as shown in Figure 8.15). Being a three-phase system, the equivalent will be of the form shown in Figure 8.16. The harmonic filters on the rectifier side of the d.c. link have been disconnected to accentuate the harmonic levels, as the presence of harmonic filters tends to mask any differences.

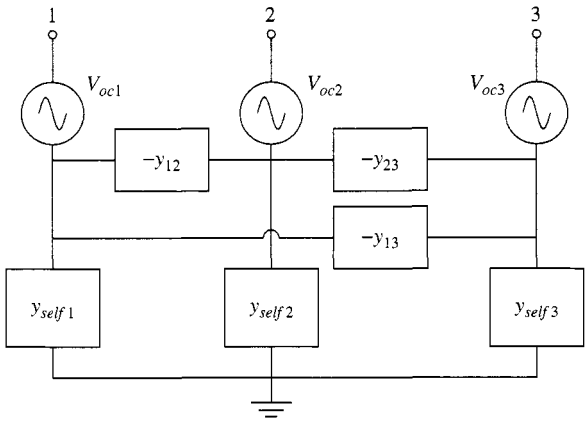

Figure 8.16. Three-phase FDNE

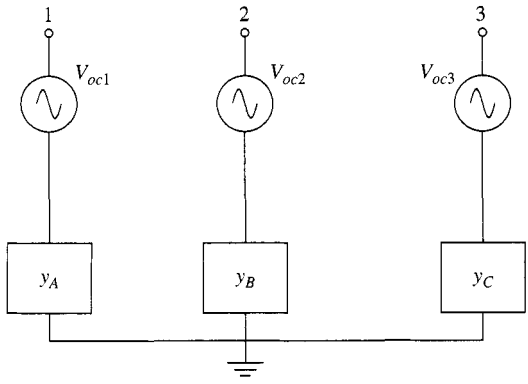

Figure 8.17 Simplified three-phase FDNE

A simplified FDNE, shown in Figure 8.17, is also considered using only the positive-sequence component. Its admittance elements are obtained by post-multiplying each 3×3 matrix by the matrix:

$$\begin{bmatrix} 1 & a^2 & a \\ a & 1 & a^2 \\ a^2 & a & 1 \end{bmatrix}$$

and then extracting the diagonal terms. This method is valid for systems with little phase current asymmetry. The effectiveness of the three FDNE equivalent alternatives is by comparison with the full representation of the system.

The first step in forming an FDNE is the calculation of the frequency response of the system to be represented. Although this is best achieved using frequency-domain programs, to enable comparison with simulations of the full system the frequency response of the test system is determined from time-domain simulations.

Figure 8.18 shows the phase voltages at the point of injection resulting from three current injection tests (at each phase of the Tiwai bus). These voltages are used to derive

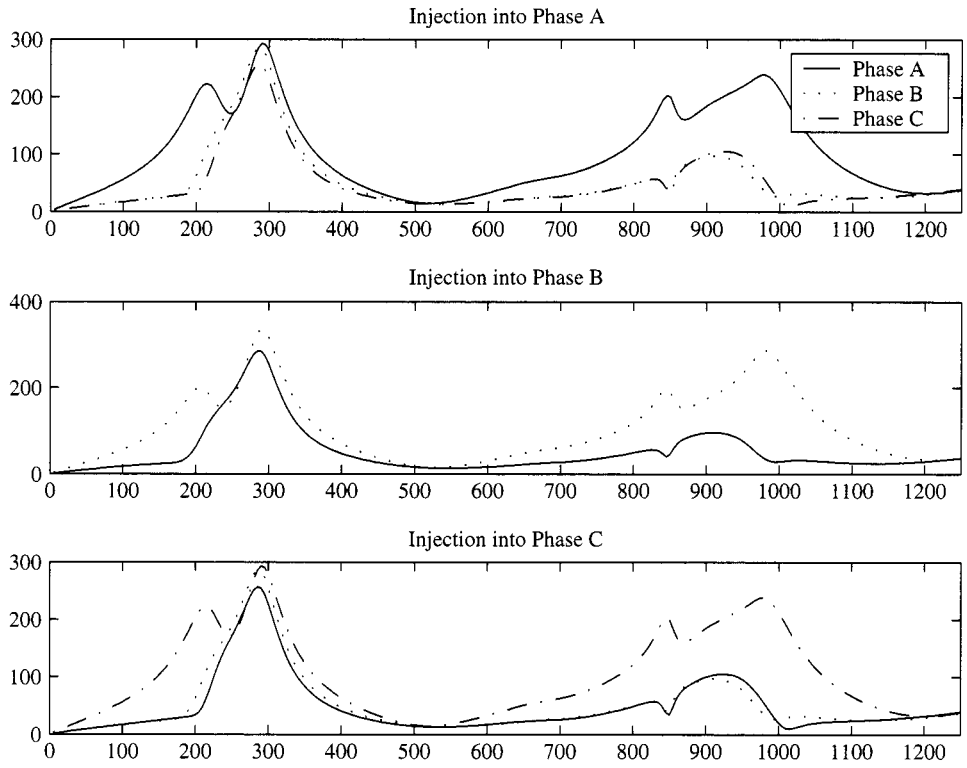

Figure 8.18 Voltages from injection tests

the self- and mutual impedances at each frequency. The 3 × 3 impedance matrices are then inverted to derive the nodal admittance matrices to be fitted (their respective magnitude and phase for the test system are shown in Figures 8.19 and 8.20).

In a nodal admittance matrix the off-diagonal elements are the negative of the interconnecting branch admittance and the diagonal terms the sum of all the branch admittances connected to a node; thus the latter are fitted by adding all admittances in the row or column (as the admittance matrices are symmetrical) of the particular node. Only six terms need to be fitted as Y_{12} and Y_{13} are the same as Y_{21} and Y_{31} respectively.

With the rational function approach each term is represented by a rational function of the form

$$H(z) = \frac{a_0 + a_1 z^{-1} + a_2 z^{-2} \cdots + a_n z^{-n}}{1 + b_1 z^{-1} + b_2 z^{-2} \cdots + b_n z^{-n}}$$

The values of the a and b coefficients are determined by setting up an over-determined system of linear equations of the form

$$\begin{bmatrix} [A_{11}] & [A_{12}] \\ [A_{21}] & [A_{22}] \end{bmatrix} \begin{pmatrix} \underline{a} \\ \underline{b} \end{pmatrix} = \begin{pmatrix} \underline{C} \\ \underline{D} \end{pmatrix}$$

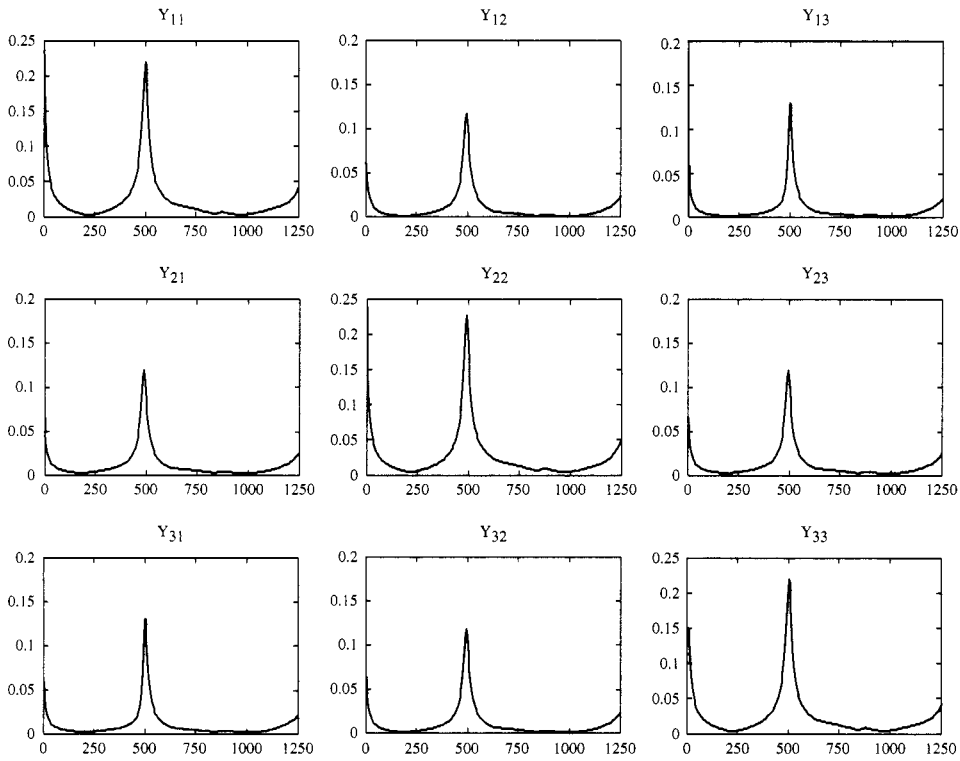

Figure 8.19 Admittance magnitude

where $\underline{a}$ and $\underline{b}$ are vectors of the a and b coefficients. $\underline{C}$ and $\underline{D}$ are vectors of the negative of the real and imaginary parts, respectively, of the sample data at each frequency. The system of linear equations is derived by evaluating the frequency response of $H(z)$ and equating to the required response at each sample point. This is solved via weighted least-squares. Two equations result from each sample point, one for the real component and the other for the imaginary component. A weighting factor of 100 is applied to equations representing the fundamental frequency so as to ensure minimal steady-state error. The rational function is implemented in PSCAD/EMTDC as a Norton equivalent (a current source with a parallel resistance). As $H(z) = I(z)/V(z)$, multiplying by the denominator and rearranging for $I(z)$ gives

$$I(z) = \underbrace{a_0 V(z)}_{\substack{\text{Instantaneous} \\ \text{term}}} + \underbrace{\left\{ \begin{array}{l} V(z)(a_1 z^{-1} + a_2 z^{-2} \cdots + a_n z^{-n}) \\ -I(z)(b_1 z^{-1} + b_2 z^{-2} \cdots + b_n z^{-n}) \end{array} \right\}}_{\text{History terms}}$$

The resistance represents the instantaneous term ($R = 1/a_0$) while the current source represents all the past history terms in current ($a_1, a_2 \ldots a_n$) and voltage ($b_1, b_2 \ldots b_n$). The complete formulation and implementation for this approach is given in [38]. The following tables contain the parameters for the model of the lower South Island of New Zealand. These have all been weighted for 50 Hz to minimize error at the fundamental.

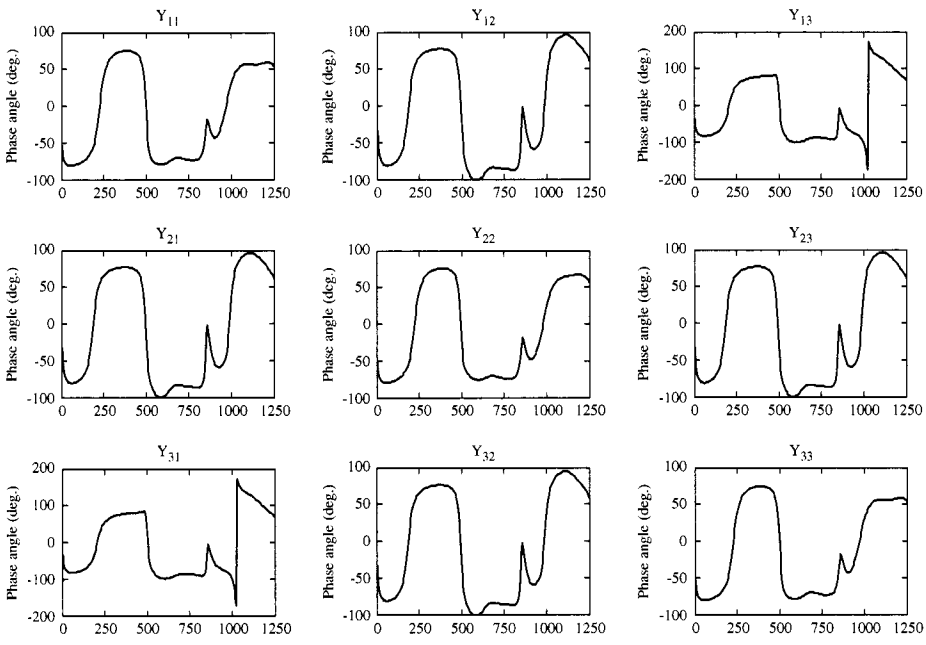

Figure 8.20 Admittance phase angle

Table 8.1 Coefficients of rational function representing Y_{self1} term

Order	Y_{self1}	
	a	*b*
0	2.4518139802491529e−003	1.0
1	−1.5523400352713717e−002	−6.6654302428731960e+000
2	4.2380331810221161e−002	1.9230399247655740e+001
3	−6.4641019199195751e−002	−3.1130273213778576e+001
4	5.9457300767762414e−002	3.0538485772657317e+001
5	−3.2959346847465210e−002	−1.8155446247494950e+001
6	1.0187297977530718e−002	6.0572751686602073e+000
7	−1.3529372195878338e−003	−8.7501014304358138e−001

The rational function forms a finally balanced system that represents the frequency response of the system. The positive and negative coefficients result in very similar numbers being subtracted and hence precision is important in the calculations. Thus a large number of decimal places is needed; this is illustrated in Tables 8.1 and 8.2 for the Y_{self1} and Y_{12} coefficients used in PSCAD/EMTDC simulation.

Rounding the coefficients to less significant digits can have a dramatic effect on the frequency response and often results in the system being unstable.

Figures 8.21 and 8.22 display the typical fitting accuracy for the Y_{12} and Y_{self1} terms respectively. The Y_{12} is fitted by an 11th order rational function while the Y_{self1} term by a 7th order. Although increasing the order of the Y_{self1} improves the fit, some poles are unstable.

Table 8.2 Coefficients of rational function representing Y_{12} term

Order	Y_{12}	
	a	*b*
0	1.9501107426634562e−003	1.0
1	−1.8984910246341156e−002	−1.0472045700750085e+001
2	8.4077491417341846e−002	5.0242749736612936e+001
3	−2.2327784954520663e−001	−1.4577147599444638e+002
4	3.9436282600293848e−001	2.8416307981056764e+002
5	−4.8528978431109171e−001	−3.9078405955678375e+002
6	4.2318006985401002e−001	3.8685683419253877e+002
7	−2.6026788334542772e−001	−2.7568394845148111e+002
8	1.0983931015277194e−001	1.3859815103973341e+002
9	−2.9928875612837458e−002	−4.6818484850277628e+001
10	4.6331885907560004e−003	9.5644565932267973e+000
11	−2.9369352575267255e−004	−8.9525681690543701e−001

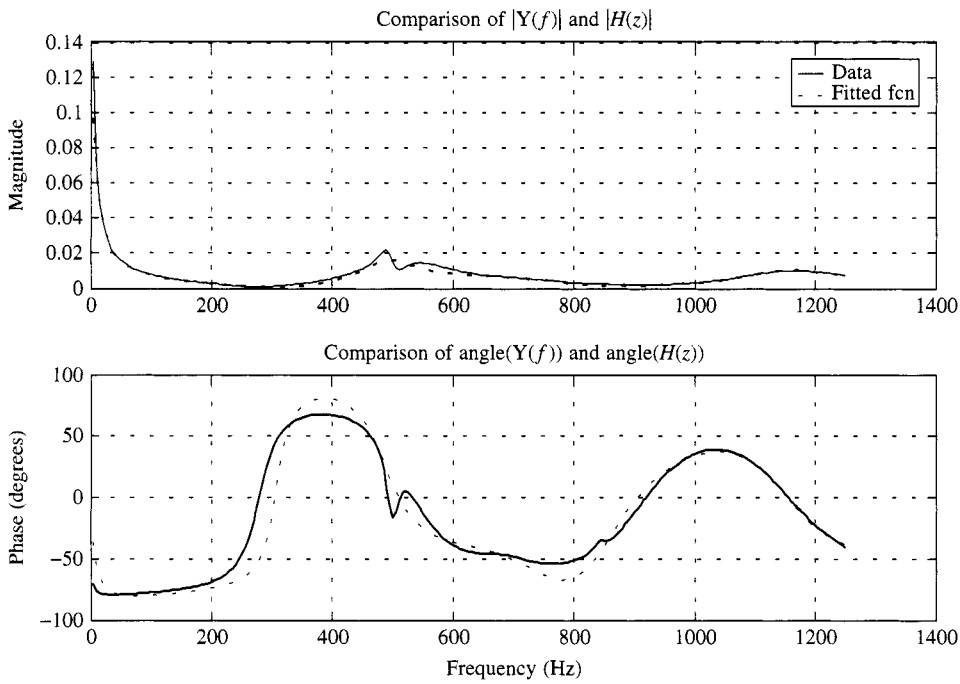

Figure 8.21 Comparison of Y_{self1} admittance term

To implement an *RLC* network, the features of the frequency response, that is the frequencies of peaks and troughs and trough magnitudes, are determined. For example, running the Y_{self1} term through a feature extraction program gives the results shown in Table 8.3.

Inspection of the frequency response allows some of the minor features to be removed, such as the 510 Hz and 545 Hz peak and trough, respectively, as these

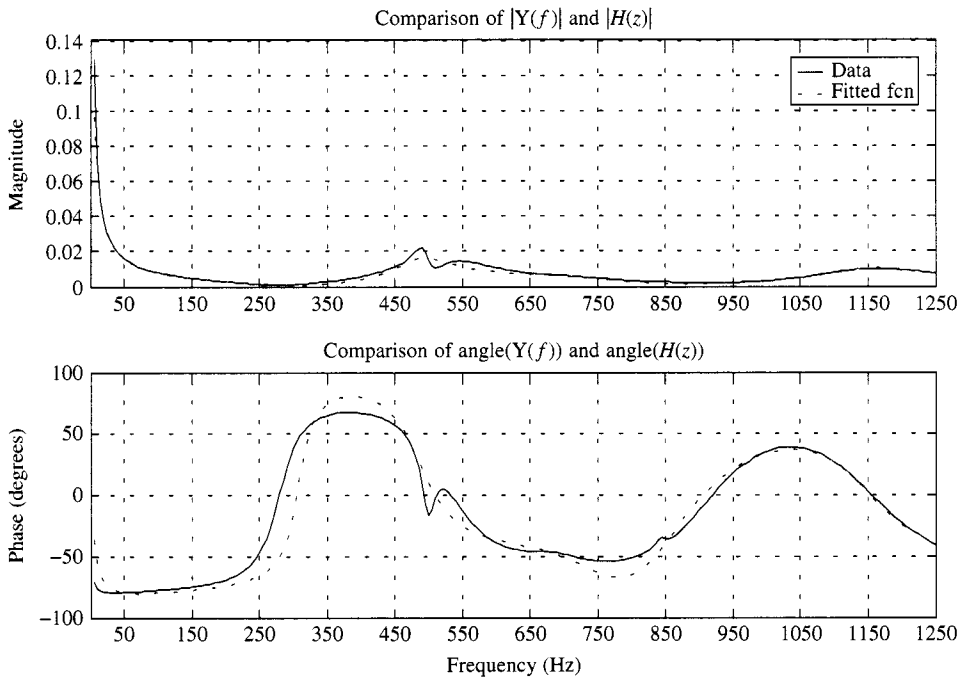

Figure 8.22 Comparison of Y_{12} admittance term

Table 8.3 Features of Y_{self1}

Frequency (Hz)	Type	Z magnitude (Ω)
280.0	Peak	1155.31
490.0	Trough	45.19
510.0	Peak	94.23
545.0	Trough	68.07
840.0	Peak	322.26
845.0	Trough	322.17
910.0	Peak	522.90
1160.0	Trough	98.09

only cause a small deviation from the overall trend. Extra peaks and troughs can be added outside the 5–1250 Hz frequency range to shape the response at the extremity of the frequency range.

The fitting procedure starts by ignoring the resistances when determining the L and C values so as to give the correct resonant frequencies. The resistances are set to be the impedance at the troughs and then all the L and C values are scaled, while maintaining the resonant frequencies, to give the correct circuit impedance at a specified match frequency. In this case the scaling frequency is 200 Hz and the match value 366.47 Ω.

The resistances of the branches are then adjusted to further improve the size of the resonant peaks. This can be achieved by modification of the impedance at the troughs

Table 8.4 Final selection of features used for Y_{self1} term

Frequency (Hz)	Type	Z magnitude Ω
0	Trough	10.0
280.0	Peak	–
490	Trough	90.18931
840.0	Peak	–
845.0	Trough	400.0
910.0	Peak	–
1160.0	Trough	98.091
1900	Peak	–

Table 8.5 Features for *RLC* FDNE (3 × 3)

		Trough frequency (Hz)	Trough magnitude (Ω)	Peak frequency (Hz)
Y_{self1}	1	0.0	10.0	280.0
	2	490	90.18931	840.0
	3	845.0	400.0	910.0
	4	1160.	98.091	1900.0
Y_{self2}	1	0.0	4.0	315.0
	2	440.0	300.0	465.0
	3	500.0	134.3544	945.0
	4	1155.0	292.0187	1900.0
Y_{self3}	1	0.0	0.1	1.0
	2	5.0	7.75	280.0
	3	490.0	90.1893	910.0
	4	1160.0	98.0910	1900.0
12	1	0.0	20.0000	185
	2	495	18.3576	845.0
	3	875	339.1000	990.0
	4	2250	5.0000	2500.0
13	1	0.0	20.000	205.0
	2	500.0	20.000	850.0
	3	880.00	300.000	1015.0
	4	1250.0	5.000	2500.0
23	1	0.0	20.000	185.0
	2	495.0	18.3576	845.0
	3	875.0	339.100	990.0
	4	2250.0	5.000	2500.0

or directly modifying the R values. Increasing the resistance effectively reduces the peak on either side. The final features used for the fitting are shown in Table 8.4. The complete set of features obtained is shown in Table 8.5. Often after this process extra branches are added to further improve the response in particular regions. The final *RLC* values obtained are given in Table 8.6, while Table 8.7 gives the matching frequency

Table 8.6 FDNE *RLC* 3 × 3

		R (Ω)	*L* (mH)	*C* (μF)
11	1	10.000	167.99566	–
	2	90.18931	94.8172641875	1.1126554076
	3	400.000	11671.3350	0.0030395291
	4	98.091	74.6789304842	0.2520729217
22	1	4.000	171.8693160074	–
	2	300.000	425.2498126926	0.3076739870
	3	134.3544	238.0594943090	0.4256128660
	4	292.018674	138.1816356405	0.1374124129
33	1	0.100	4205.3875120966	–
	2	7.750	175.2641568245	5781.0556064702
	3	90.18931	94.3575961209	1.1180757678
	4	98.091	76.6775418608	0.2455026041
12	1	20.000	311.0932318150	–
	2	18.3576	66.3414891513	1.5582769607
	3	339.100	1660.0376649282	0.0199299503
	4	5.000	9.2106855866	0.5432294040
	5	2000.00	4300.0	0.1720726
13	1	20.000	383.6827097296	–
	2	20.000	89.0417534485	1.1379064284
	3	300.000	1305.8401298774	0.0250486837
	4	5.000	94.3258081564	0.1718658944
	5	2000.000	3881.828	0.1552731
23	1	20.000	311.0932318150	–
	2	18.35760	66.3414891513	1.5582769607
	3	339.100	1660.0376649282	0.0199299503
	4	5.000	9.2106855866	0.5432294040
	5	2000.000	4300.00	0.1720726

Table 8.7 Match frequency and values

Term	Match frequency (Hz)	Match magnitude (Ω)
Y_{self1}	200.0	366.47
Y_{self2}	200.0	300.47
Y_{self3}	200.0	366.47
Y_{12}	140.0	600.0
Y_{13}	100.0	305.0
Y_{23}	140.0	600.0

and magnitude. Note that terms Y_{12}, Y_{13} and Y_{23} have an extra branch added (i.e. five *RLC* branches and yet there are only four peak/trough combinations) to improve the response at the first parallel resonance (approximately 185 Hz). Figures 8.23 and 8.24 display the comparison between the FDNE and required response.

Assuming balanced phase currents and diagonalising the impedance matrices results in three uncoupled frequency responses, each of which can be fitted with an *RLC* circuit. Applying the same procedure of feature extraction and synthesis of the *RLC*

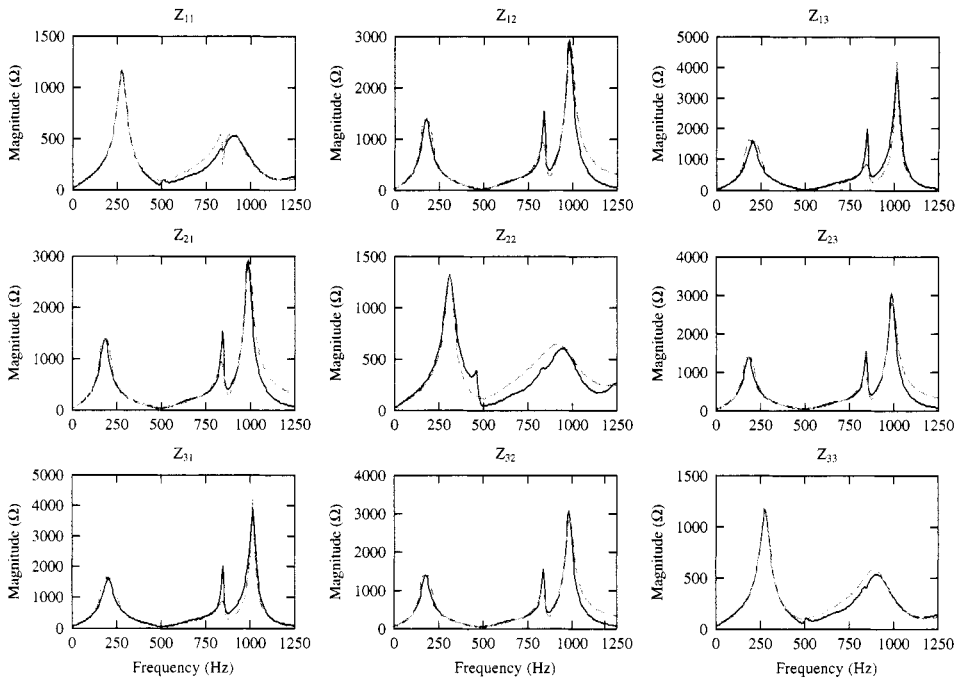

Figure 8.23 Comparison of magnitude response (*RLC* 3 × 3 FDNE)

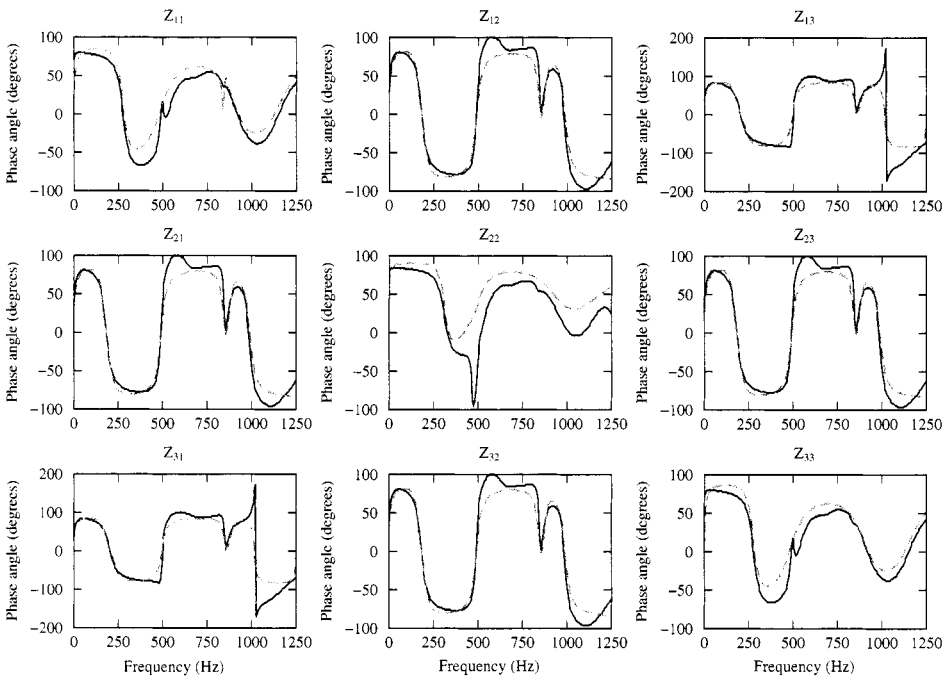

Figure 8.24 Comparison of phase angle response (*RLC* 3 × 3 FDNE)

circuit results in the values shown in Table 8.8. Each phase has a correction branch (branch 5 for phases A and C, and branch 6 for phase B) designed to give a better match at fundamental frequency (50 Hz). These branches are series resonant at 45 Hz, so at 50 Hz the impedance magnitude and phase angle are far closer to what is required. Figure 8.25 displays the match for the phase A term. A better match can be achieved by adding more branches to shape the response even further, particularly between 800 Hz and 1000 Hz.

Table 8.8 FDNE, *RLC* simplified

		R (Ω)	L (mH)	C (μF)
A	1	30.000	74.838	–
	2	1.400	21.554	4.8549
	3	91.30	1167.1335	0.068249
	4	10.00	15.296	0.9799
	5	5.0	530.5	23.58
B	1	30.000	74.072	–
	2	89.700	77.518	0.45837
	3	4.0	21.825	4.6423
	4	65.4	463.24	0.072409
	5	10.0	14.684	1.0207
	6	5.0	530.5	23.58
C	1	35.000	68.236	–
	2	7.000	19.959	5.1795
	3	40.000	36.513	0.090611
	4	10.000	13.795	1.0865
	5	1.0	530.5	23.58

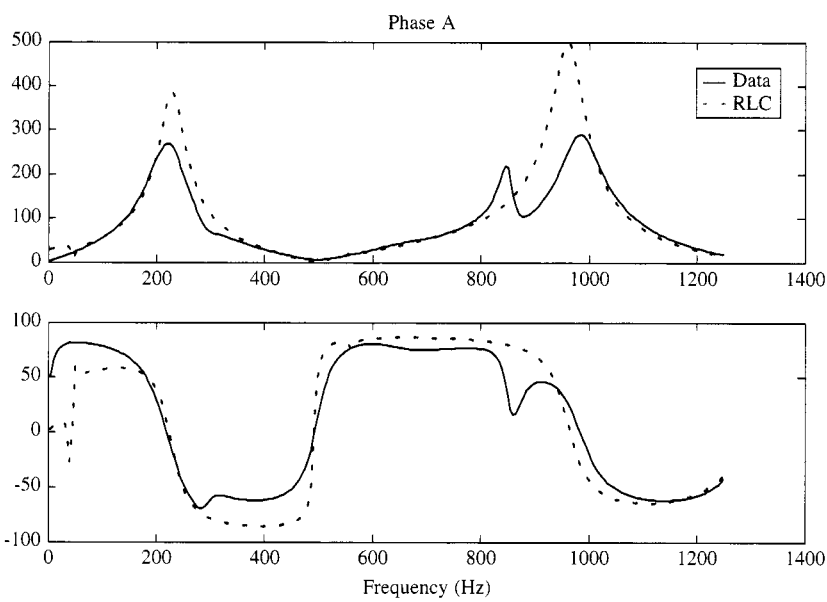

Figure 8.25 Phase A term after diagonalising

Table 8.9 FDNE voltage source parameters

	Voltage (phase to neutral)	
	Magnitude (kV)	Phase angle (degrees)
Phase A	121.599	61.16755
Phase B	121.599	−59.15545
Phase C	121.599	180.66100

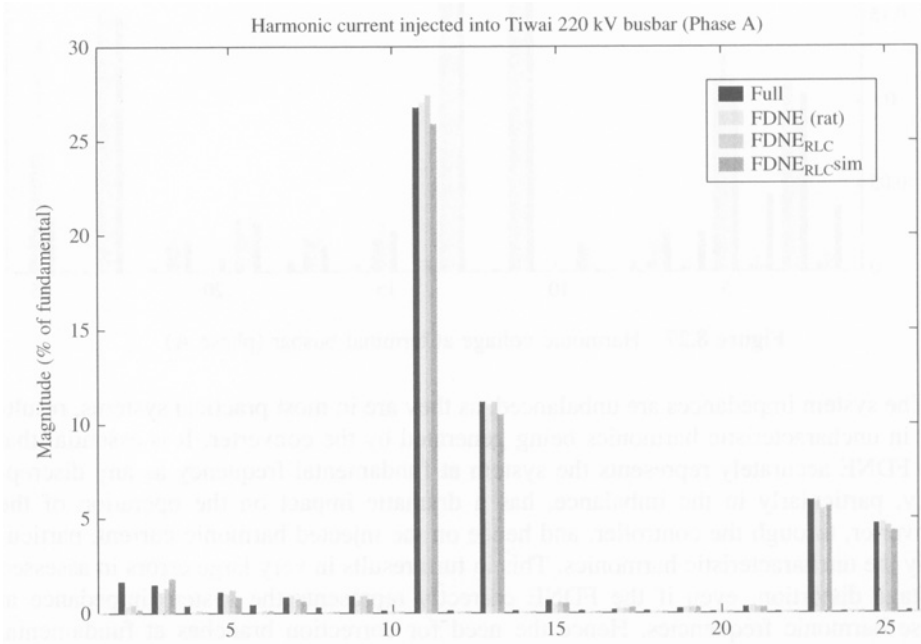

Figure 8.26 Harmonic current injection (phase A)

The voltage source magnitude and phase angle for all the FDNEs are set to be that of the full system under open circuit. These values are given in Table 8.9.

Setting the rectifier α order to 0.6 radians and inverter order to 2.42 and simulating the four cases (full, FDNE rational functions, FDNE *RLC* and FDNE *RLC* simplified) give the results displayed in Figures 8.26 and 8.27. This example shows that the assessed injected current from the d.c. link is very close for all cases. The harmonic levels predicted by the FDNE (rational function) match the full system best. The injected current into the rectifier a.c. system by the HVd.c. link is similar, with the rational function FDNE being the most accurate and the simplified *RLC* the worst. The RLC FDNE circuits show a large discrepancy in the 25th harmonic on the terminal voltage, which does not appear in the injected current. This is understandable when the fitting errors are considered (Figure 8.23 for the *RLC* FDNE and Figure 8.25 for the simplified *RLC* FDNE).

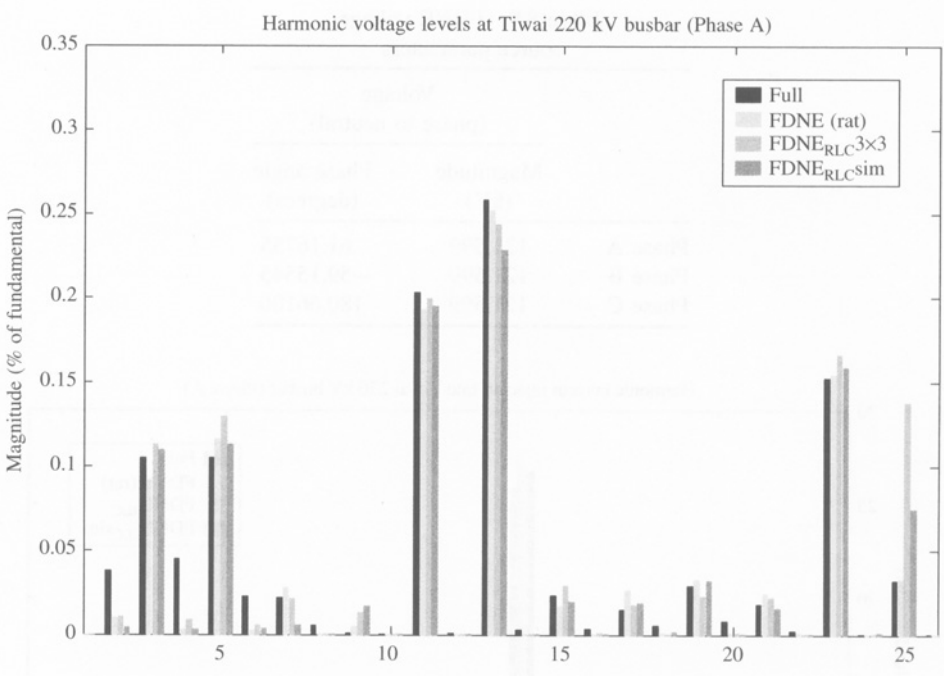

Figure 8.27 Harmonic voltage at terminal busbar (phase A)

The system impedances are unbalanced, as they are in most practical systems, resulting in uncharacteristic harmonics being generated by the converter. It is essential that the FDNE accurately represents the system at fundamental frequency as any discrepancy, particularly in the imbalance, has a dramatic impact on the operation of the converter, through the controller, and hence on the injected harmonic current, particularly the uncharacteristic harmonics. This in turn results in very large errors in assessed voltage distortion, even if the FDNE correctly represents the system impedance at these harmonic frequencies. Hence the need for correction branches at fundamental frequency for *RLC* FDNE or weighting factors for the rational function approach. Tables 8.10 and 8.11 show the fundamental frequency conditions for this comparison. Getting the fundamental frequency matching right is more important than getting the matching correct at harmonic frequencies.

If the interaction of a nonlinear device with the a.c. system is not modelled; that is, the device is represented by a fixed current injection, then the assessed harmonic

Table 8.10 Fundamental phase-neutral voltage at Tiwai 220 kV busbar

	Full		FDNE (rational fcn)		*RLC* 3 × 3		*RLC* (simplified)	
	Magnitude (kV)	Angle (degrees)	Magnitude (kV)	Angle (degrees)	Magnitude (kV)	Angle (degrees)	Magnitude (kV)	Angle (degrees)
Phase A	120.208	−27.48	120.183	−28.25	120.280	−28.22	120.411	−27.99
Phase B	120.551	−147.82	120.558	−148.45	120.678	−148.44	120.678	148.26
Phase C	119.804	92.14	120.133	91.44	120.247	91.45	120.343	91.64

Table 8.11 Fundamental current injected into Tiwai 220 kV busbar

	Full		FDNE (rational fcn)		*RLC* 3 × 3		*RLC* (simplified)	
	Magnitude (kA)	Angle (degrees)	Magnitude (kA)	Angle (degrees)	Magnitude (kA)	Angle (degrees)	Magnitude (kA)	Angle (degrees)
Phase A	0.060	−87.19	0.060	−85.90	0.060	−85.32	0.060	−85.90
Phase B	0.056	154.02	0.054	151.78	0.053	151.51	0.054	151.78
Phase C	0.057	26.89	0.059	26.09	0.060	25.71	0.059	26.09

levels given by the FDNE will be even closer to the full system run under the same conditions. The only difference will be the fitting errors. This provides one method for finding modelling errors, by performing injection tests on the FDNE model in the EMTP-type program, then taking the FFT to obtain the frequency response and comparing it to the matched response in the frequency domain.

Although the modelling of the frequency dependency of overhead lines and cables is well advanced in EMTP packages, this is not true for the other components. The standard models for generators, transformers and loads do not represent the increase in resistance (or slight reduction in inductance) associated with skin effect. This increase in resistance will be most noticeable when a resonance occurs. Hence, using a frequency-domain program to obtain the frequency response of the a.c. system to be represented by an FDNE will give a frequency response closer to reality. Having developed an FDNE from frequency data obtained using a frequency-domain program, it is very hard to verify the accuracy of the final FDNE without accurate measurements of the actual system. Hence, the above approach of using the less accurate time-domain derivation of frequency data has been used, as this allows the complete time-domain model to be used as the benchmark. Improved representation of components and their frequency dependency can be achieved by using *RL* networks, as illustrated in Figure 8.28 for a generator.

Figures 8.29–8.31 display the impedance magnitude, phase angle and impedance loci, respectively, for frequency-domain and time-domain generation of frequency responses. Frequency-dependent transmission line models with standard generator, transformer and load models were used in the time domain. As expected, there is reasonable agreement except at resonance, where the frequency domain generates a higher peak. The impedance loci look a lot worse, as the impedance changes very fast with frequency, near resonances. Hence the loops represent very narrow frequency bands and are the regions where discrepancies in resistances are most pronounced.

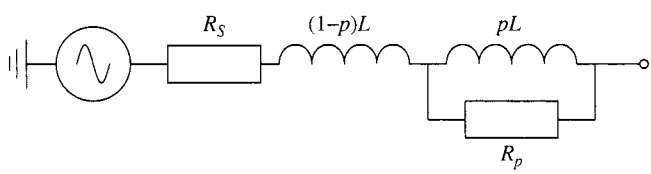

Figure 8.28 Generator model with improved frequency response

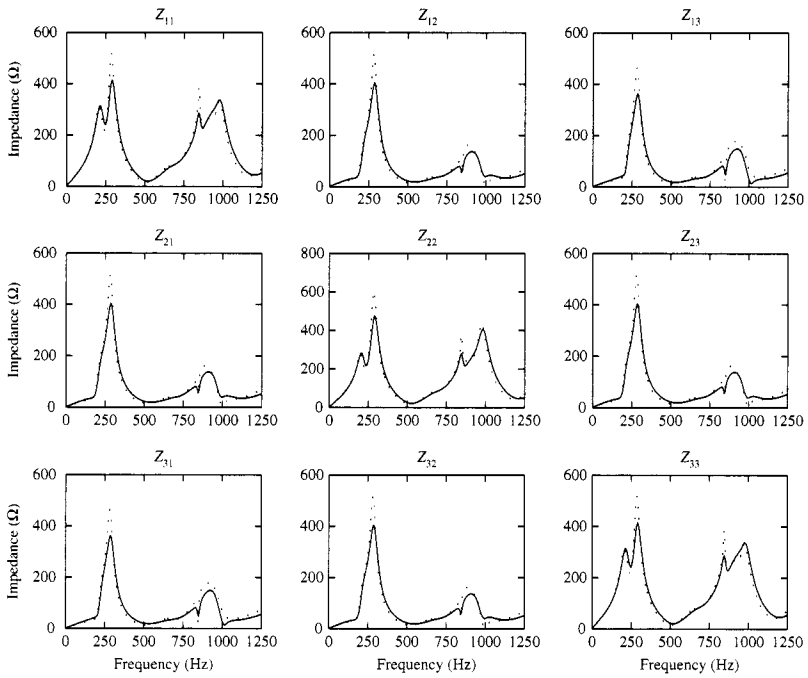

Figure 8.29 Comparison between (———) time- and (· · · · · ·) frequency-domain assessment of system impedance

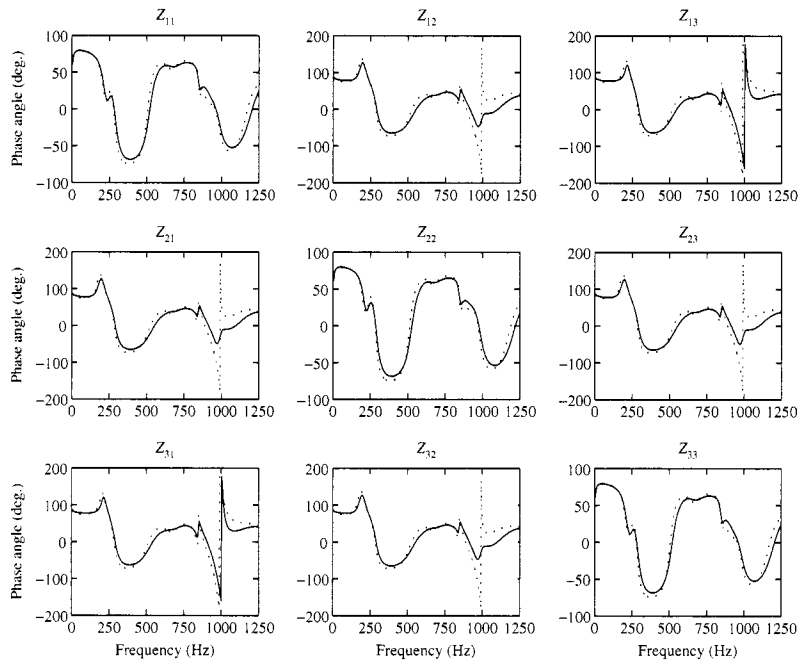

Figure 8.30 Comparison between (———) time- and (· · · · · ·) frequency-domain assessment of system impedance

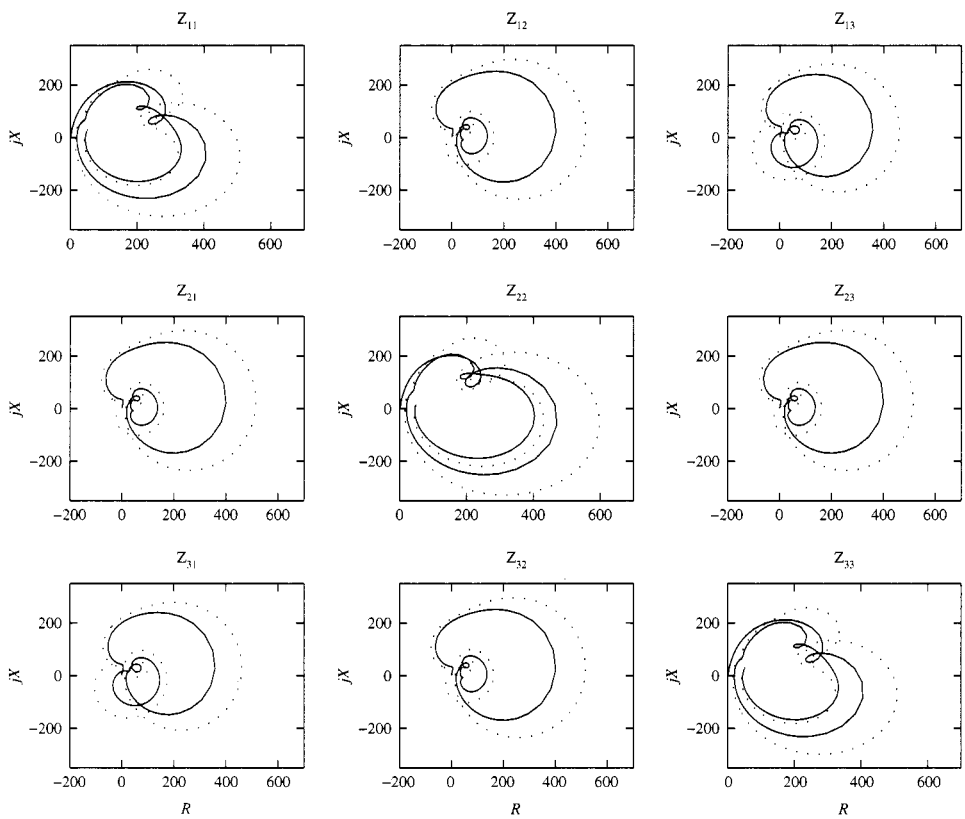

Figure 8.31 Comparison between (———) time- and (· · · · · ·) frequency-domain assessment of system impedance

8.7 Discussion on Advanced Harmonic Modelling

Three advanced methods have been described in this chapter for the simulation of the power system harmonic sources. These are the harmonic domain, the time domain and a hybrid combination of the conventional frequency and time domains.

The harmonic domain includes a linearised representation of the nonlinear components around the operating point in a full Newton solution. The fundamental frequency load flow is also incorporated in the Newton solution, which thus provides the ideal tool for general steady-state assessment. However, the complexity of the formulation to derive the system Jacobian may well prevent its final acceptability.

The hybrid proposal takes advantage of the characteristics of the frequency and time domains for the linear and nonlinear components, respectively. The hybrid algorithm is conceptually simpler and more flexible than the harmonic domain but it is not a full newton solution and therefore not as reliable under weak system conditions.

The direct time-domain solution, using EMTP-type programs, can be used for the derivation of the steady-state voltage and current waveforms and harmonics levels, and is particularly good at taking into account complex nonlinear devices and their controllers. Care is required to ensure a realistic resistance at harmonic frequencies.

FDNE can be used to represent the arbitrary frequency response of an a.c. system. When representing the interaction between the a.c. system and nonlinear devices, an accurate match at fundamental frequency must be achieved otherwise the incorrect operating conditions will result, with wrong harmonic injection estimates being obtained. This will follow through to wrong harmonic voltages.

With fixed harmonic current injections only the match at harmonic frequencies is important.

The rational function representation is more accurate and more methodical than the fitting of *RLC* networks, as the latter requires a certain amount of manual tuning of parameters. However, the rational function approach has the problem of stability, and hence trial and error is usually required to find the highest order that is stable.

8.8 References

1. Dickmander, D.L., Lee, S.Y., Desilets, G.L. and Granger, M. (1994) AC/DC harmonic interactions in the presence of GIC for the Quebec–New England phase II HVdc transmission, *IEEE Trans. Power Delivery*, **9**(1), 68–78.
2. Hammad, A.E. (1992) Analysis of the second harmonic instability for the Chateauguay HVdc/svc scheme, *IEEE Trans. Power Delivery*, **7**(1), 410–15.
3. Arrillaga, J., Smith, B.C., Watson, N.R. and Wood, A.R. (1997) *Power System Harmonic Analysis*, John Wiley & Sons, Chichester.
4. Yacamini, R. and De Oliveira, J.C. (1980) Harmonics in multiple converter systems: a generalised approach, *Proc. IEE*, **127**(2), 96–106.
5. Reeve, J. and Baron, J.A. (1971) Harmonic interaction between HVdc converters and a.c. power systems, *IEEE Trans. Power Apparatus and Systems*, **90**(6), 2785–93.
6. Callaghan, C. and Arrillaga, J. (1989) A double iterative algorithm for the analysis of power and harmonic flows at a.c.–d.c. terminals, *Proc. IEE*, **136**(6), 319–24.
7. Semlyen, A., Acha, E. and Arrillaga, J. (1992) Newton-type algorithms for the harmonic phasor analysis of non-linear power circuits in periodical steady state with special reference to magnetic non-linearities, *Trans. IEEE Power Delivery*, **PWRD-7**(3), 1090–8.
8. Semlyen, A. and Medina, A. (1995) Computation of the periodic steady state in system with non-linear components using a hybrid time and frequency domain methodology, *Trans. IEEE Power Systems*, **10**(3), 1498–1504.
9. Usaola, J. and Mayordomo, J.G. (1994) Multifrequency analysis with time domain simulation, *ETEP*, **6**(1), 53–9.
10. Usaola, J. and Mayordomo, J.G. (1990) Fast steady state technique for harmonic analysis, *ICHQP IV*, Budapest, pp. 336–42.
11. Semlyen, A. and Shlash, M. (2000) Principles of modular harmonic power flow methodology, *Proc. IEE Gener. Transm. Distrib.*, **147**(1), 1–6.
12. Smith, B.C., Watson, N.R., Wood, A.R. and Arrillaga, J. (1995) Steady state model of the ac-dc converter in the harmonic domain, *Proc. IEE Gener. Transm. Distrib.*, **142**(2), 109–18.
13. Bathurst, G.N., Watson, N.R. and Arrillaga, J. (2000) Adaptive frequency-selection method for a Newton solution of harmonics and inter-harmonics, *Proc. IEE Gener. Transm. Distrib.*, **142**(2), 126–30.
14. Arrillaga, J., Bathurst, G.N. and Watson, N.R. (2001) Adaptive derivation of inter-harmonics in variable speed drives, EPE 2001 Conference, Gratz, Austria.
15. Xia, D. and Heydt, G.T. (1982) Harmonic power flow studies, Part I—Formulation and solution, Part II—Implementation and practical application, *IEEE Trans. Power Apparatus Systems*, **PAS-101**, 1257–70.

16. Arrillaga, J. and Callaghan, C.D. (1991) Three-phase a.c.–d.c. load and harmonic flows, *IEEE Trans. Power Delivery*, **6**(1), 238–44.
17. Xu, W., Marti, J.R. and Dommel, H.W. (1991) A multiphase harmonic load flow solution technique, *IEEE Trans. Power Apparatus and Systems*, **PS-6**, 174–82.
18. Valcarcel, M. and Mayordomo, J.G. (1993) Harmonic power flow for unbalanced systems, *IEEE Trans. Power Delivery*, **8**(4), 2052–9.
19. Bathurst, G.N., Smith, B.C., Watson, N.R. and Arrillaga, J. (2000) A modular approach to the solution of the three-phase harmonic power flow, *IEEE Trans. Power Delivery*, **15**(3), 984–9.
20. Arrillaga, J., Acha, E., Densem, T. and Bodger, P.S. (1986) Ineffectiveness of transmission line transpositions at harmonic frequencies, *Proc. IEE*, **133C**(2), 99–104.
21. Harker, B.J. and Arrillaga, J. (1979) Three-phase a.c.–d.c. load flow, *Proc. IEE*, **126**(12), 1275–81.
22. Arrillaga, J. and Watson, N.R. (2001) *Computer Modelling of Electrical Power Systems*, John Wiley & Sons, Chichester.
23. Szetchman, M., Weiss, T. and Thio, C.V. (1991) First benchmark model for HVdc control studies, *Electra*, **135**, 55–75.
24. Heydt, G.T. (1989) Identification of harmonic sources by a state estimation technique, *IEEE Trans. Power Delivery*, **4**(1), 569–76.
25. Arrillaga, J., Watson, N.R. and Chen, S. (2000) *Power System Quality Assessment*, John Wiley & Sons, Chichester.
26. Beides, H.M. and Heydt, G.T. (1991) Dynamic state estimation of power system harmonics using Kalman filter methodology, *IEEE Trans. Power Delivery*, **6**(4), 1663–70.
27. Meliopoulos, A.P.S., Zang, F. and Zellingher, S. (1994) Power system harmonic state estimation, *IEEE Trans. Power Delivery*, **9**(3), 1701–9.
28. Du, Z.P., Arrillaga, J. and Watson, N.R. (1996) Continuous harmonic state estimation of power systems, *Proc. IEE*, **143 Pt.C**(4), 329–36.
29. Du, Z.P., Arrillaga, J. and Watson, N.R. (1996) A new symbolic method of observability analysis for harmonic state estimation of power systems, *Proc. IEE*, **1**, 431–5.
30. Farach, J.E., Grady, W.M. and Arapostathis, A. (1996) Optimal harmonic sensor placement in fundamental network topologies, *Proc. IEE Gener. Transm. Distrib.*, **143**(6), 608–12.
31. Ma, H. and Grigis, A.A. (1996) Identification and tracking of harmonic sources in a power system using a Kalman filter, *IEEE Trans. Power Delivery*, **11**(3), 1659–65.
32. Hartana, R.K. and Richards, G.G. (1990) Harmonic source monitoring and identification using neural network, *IEEE Trans. Power Systems*, **5**(4), 1098–104.
33. Soliman, S.A., Christensen, G.S., Kelly, D.H. and El-Naggar, K.M. (1990) A state estimation algorithm for identification and measurement of power system harmonics, *Electric Power Research*, no. 19, 195–206.
34. Osowski, S. (1994) SVD technique for estimation of harmonic components in a power system: a statistical approach, *Proc. IEE Gener., Transm. Distrib.*, **141**(5), 473–9.
35. Moo, C.S. and Chang, Y.N. (1995) Group-harmonic identification in power systems with non-stationary waveforms, *Proc. IEE Gener., Transm. Distrib.*, **142**(5), 517–22.
36. Hingorani, N.G. and Burbury, M. (1970) Simulation of ac system impedance in HVdc system studies, *IEEE Trans. Power Apparatus Systems*, **89**(5/6), 820–8.
37. Watson, N.R. and Arrillaga, J. (1988) Frequency-dependent ac system equivalents for harmonic studies and transient converter simulation, *Trans. IEEE*, **PD-3**(3), 1196–1203.
38. Watson, N.R. and Arrillaga, J. (2003) Power systems electromagnetic transients simulation, IEE Power and energy series 39, London.